

# UCLA

## UCLA Previously Published Works

### Title

Mussel-Inspired Multifunctional Hydrogel Coating for Prevention of Infections and Enhanced Osteogenesis.

### Permalink

<https://escholarship.org/uc/item/3h37w45s>

### Journal

ACS applied materials & interfaces, 9(13)

### ISSN

1944-8244

### Authors

Cheng, Hao

Yue, Kan

Kazemzadeh-Narbat, Mehdi

et al.

### Publication Date

2017-04-01

### DOI

10.1021/acsami.6b16779

Peer reviewed

## Article

**Mussel-Inspired Multifunctional Hydrogel Coating for Prevention of Infections and Enhanced Osteogenesis**

Hao Cheng, Kan Yue, Mehdi Kazemzadeh-Narbat, Yanhui Liu, Akbar Khalilpour, Bingyun Li, Yu Shrike Zhang, Nasim Annabi, and Ali Khademhosseini

*ACS Appl. Mater. Interfaces*, **Just Accepted Manuscript** • DOI: 10.1021/acsami.6b16779 • Publication Date (Web): 31 Jan 2017Downloaded from <http://pubs.acs.org> on February 1, 2017**Just Accepted**

“Just Accepted” manuscripts have been peer-reviewed and accepted for publication. They are posted online prior to technical editing, formatting for publication and author proofing. The American Chemical Society provides “Just Accepted” as a free service to the research community to expedite the dissemination of scientific material as soon as possible after acceptance. “Just Accepted” manuscripts appear in full in PDF format accompanied by an HTML abstract. “Just Accepted” manuscripts have been fully peer reviewed, but should not be considered the official version of record. They are accessible to all readers and citable by the Digital Object Identifier (DOI®). “Just Accepted” is an optional service offered to authors. Therefore, the “Just Accepted” Web site may not include all articles that will be published in the journal. After a manuscript is technically edited and formatted, it will be removed from the “Just Accepted” Web site and published as an ASAP article. Note that technical editing may introduce minor changes to the manuscript text and/or graphics which could affect content, and all legal disclaimers and ethical guidelines that apply to the journal pertain. ACS cannot be held responsible for errors or consequences arising from the use of information contained in these “Just Accepted” manuscripts.



# Mussel-Inspired Multifunctional Hydrogel Coating for Prevention of Infections and Enhanced Osteogenesis

Hao Cheng,<sup>a,b,c,#</sup> Kan Yue,<sup>a,b,#</sup> Mehdi Kazemzadeh-Narbat,<sup>a,b,#</sup> Yanhui Liu,<sup>a,b,d</sup> Akbar Khalilpour,<sup>a,b</sup> Bingyun Li,<sup>e</sup> Yu Shrike Zhang,<sup>a,b</sup> Nasim Annabi,<sup>a,b,f,\*</sup> Ali Khademhosseini<sup>a,b,g,h,\*</sup>

<sup>a</sup> Biomaterials Innovation Research Center, Division of Biomedical Engineering, Department of Medicine, Brigham and Women's Hospital, Harvard Medical School, Cambridge, MA, 02139, USA

<sup>b</sup> Harvard-MIT Division of Health Sciences and Technology, Massachusetts Institute of Technology, Cambridge, MA, 02139, USA

<sup>c</sup> Orthopaedic Department, Tongji Hospital, Tongji Medical College, Huazhong University of Science and Technology, Wuhan 430030, China

<sup>d</sup> College of Textiles, Donghua University, Shanghai, 201620, China

<sup>e</sup> Department of Orthopaedics, School of Medicine, West Virginia University, Morgantown, WV 26506, USA

<sup>f</sup> Department of Chemical Engineering, Northeastern University, Boston, MA, 02115-5000, USA

<sup>g</sup> Department of Bioindustrial Technologies, College of Animal Bioscience and Technology, Konkuk University, Seoul, 143-701, the Republic of Korea

<sup>h</sup> Department of Physics, King Abdulaziz University, Jeddah, 21569, Saudi Arabia

# These authors contributed equally to this work.

\* Corresponding authors: Prof. Ali Khademhosseini ([alik@bwh.harvard.edu](mailto:alik@bwh.harvard.edu)), Prof. Nasim Annabi ([n.annabi@neu.edu](mailto:n.annabi@neu.edu))

**Keywords:** Adhesive hydrogels; titanium implant; antimicrobial; osteogenesis; silicate nanoparticles

**Abstract.**

Prevention of post-surgery infection and promotion of bio-integration are the key factors to achieve long-term success in orthopaedic implants. Localized delivery of antibiotics and bioactive molecules by the implant surface serves as a promising approach towards these goals. However, previously reported methods for surface functionalization of the titanium (Ti) alloy implants to load bioactive ingredients suffer from time-consuming complex processes and lack of long-term stability. Here, we present the design and characterization of an adhesive, osteoconductive, and antimicrobial hydrogel coating for Ti implants. To form the multifunctional hydrogels, a photocrosslinkable gelatin-based hydrogel was modified with catechol motifs to enhance adhesion to Ti surfaces and thus promote coating stability. To induce antimicrobial and osteoconductive properties, a short cationic antimicrobial peptide (AMP) and synthetic silicate nanoparticles (SNs) were introduced into the hydrogel formulation. The controlled release of AMP loaded in the hydrogel demonstrated excellent antimicrobial activity to prevent biofilm formation. Moreover, the addition of SNs to the hydrogel formulation showed enhanced osteogenesis when cultured with human mesenchymal stem cells, suggesting the potential to promote new bone formation in the surrounding tissues. Considering the unique features of our implant hydrogel coating including high adhesion, antimicrobial capability, and the ability to induce osteogenesis, it is believed that our design provides a useful alternative method for bone implant surface modification and functionalization.

## 1. Introduction

Orthopaedic implants based on titanium (Ti) or Ti alloys have been extensively used in clinics due to their superior mechanical characteristics and biocompatibility.<sup>1-3</sup> However, the long-term usage of implants is often compromised due to persistent infections post-surgery, which are challenging to treat and could eventually lead to replacement of the prostheses.<sup>4,5</sup> Controlled localized delivery of certain antibiotics loaded in the coating layer of the implants has been proposed as a promising strategy to prevent implant-associated infections and failure. Several different methods have been reported to introduce antibiotics on the surface of the implants. For example, silver nanoparticles have been loaded on implant surfaces to provide antimicrobial activities.<sup>6,7</sup> Moreover, a short cationic antimicrobial peptide (AMP) known as HHC-36 has also been investigated as an antimicrobial component for Ti implant surface modification, due to its wide-spectrum antimicrobial activity against common Gram-positive and Gram-negative bacteria with enhanced efficacy compared to traditional antibiotics.<sup>8-11</sup> However, these reported methods are generally time-consuming and require complex multistep procedures to achieve surface modification and drug loading.<sup>6,9,10,12,13</sup>

Another important requirement for successful long-term bone implant is the proper osteointegration between the implant and the surrounding tissues.<sup>14</sup> Although it has been demonstrated that cells can adhere and spread on Ti substrates with a TiO<sub>2</sub> layer, Ti metals are generally considered bioinert. As a result, introduction of bioactive molecules on Ti surfaces has been explored to enhance cell functions, to direct new tissue formation, and to promote bio-integration.<sup>15,16</sup> Previously, many different bioactive ingredients have been used for the surface modification of Ti implants to promote tissue integration and healing. For example, the introduction of Arg-Gly-Asp (RGD) short peptide could enhance adhesion and function of osteoblasts.<sup>17</sup> Besides, the immobilization of inorganic nanoparticles,<sup>15</sup> growth factors,<sup>15,18</sup> and microRNA-loaded nanocapsules<sup>19</sup> has been shown to enhance bone regeneration.

1  
2 For clinical applications, it would be ideal to achieve the surface modification of Ti implants by simple  
3  
4 procedures, for example, spraying a drug-loading solution onto the implant immediately before the surgery,  
5  
6 which can form a coating layer strongly binding to the implant *in situ* with enhanced coating stability. It is  
7  
8 also preferred to be able to simultaneously load multiple bioactive components with different physical  
9  
10 characteristics (such as peptides and inorganic nanoparticles) on Ti surfaces within a single modification  
11  
12 step. This will allow feasible introduction of different functions (e.g., antimicrobial activities, motifs for cell  
13  
14 adhesion, growth factors to direct cell differentiation, etc.) and subsequent optimization of potential  
15  
16 synergetic positive effects from each component. Up to now, it is still quite challenging to achieve these  
17  
18 goals.  
19  
20  
21  
22  
23

24  
25 Chemically crosslinked hydrogels could serve as the matrix for the surface modification, given their  
26  
27 insolubility to resist washing away by body fluids. In particular, photocrosslinkable hydrogels provide the  
28  
29 option to first spray the prepolymer solution onto the implants, followed by *in situ* photocrosslinking to cure  
30  
31 the coating layer.<sup>12,20,21</sup> However, to achieve long-term stability, hydrogels should possess strong adhesion to  
32  
33 Ti surfaces, especially under wet environments. Inspired by the unusual ability of mussels to adhere to  
34  
35 essentially any surfaces under water, extensive studies in the past few decades suggest that the presence of  
36  
37 catechol motifs contributes to adhesion improvement.<sup>22,23</sup> Since then, mussel-inspired biomaterials have  
38  
39 been extensively studied for various applications, including developing a general coating strategy,<sup>24</sup>  
40  
41 designing strong adhesives under wet conditions,<sup>25,26</sup> fabricating hybrid composite nanoparticles,<sup>27</sup> among  
42  
43 many others.<sup>28-30</sup> In particular, mussel-inspired hydrogels have been demonstrated with unique properties,  
44  
45 such as highly adhesive, self-healing, pollutant absorbing, and anti-fouling.<sup>30</sup> Especially, in the case of  
46  
47 surface modification of inorganic Ti implants, the unique strong and reversible coordination bonds between  
48  
49 Ti atoms and the catechol motifs could further enhance the binding strength.<sup>23</sup> Recently, catechol-containing  
50  
51 synthetic polymers have been demonstrated to form adhesive coating layers on metal substrates following  
52  
53  
54  
55  
56  
57  
58  
59  
60

1  
2 simple spin-coating techniques,<sup>31</sup> which can be used as load-bearing glues at the metal-plastic interfaces.

3  
4 To combine the desirable features such as easy application, antimicrobial activity, and regenerative  
5  
6 capability, we propose to develop an mussel-inspired, adhesive and biocompatible hydrogel coating that can  
7  
8 be crosslinked *in situ* after spraying onto the implant surfaces.<sup>30</sup> Antimicrobial drugs and other bioactive  
9  
10 ingredients can be physically loaded into this hydrogel matrix to achieve controlled delivery after surgeries.

11  
12 We proposed to use gelatin methacryloyl (GelMA), which has been popularized in the field of tissue  
13  
14 engineering and regenerative medicine,<sup>16,32-34</sup> as a regenerative hydrogel material. Further functionalization  
15  
16 of GelMA hydrogels with catechol motifs can enhance the binding affinity with Ti surfaces. To introduce  
17  
18 antimicrobial activity, we selected the AMP to be loaded into the hydrogel with controlled release  
19  
20 capability.<sup>8-11</sup> Moreover, we added osteoconductive silicate nanoparticles (SNs), commercially available as  
21  
22 Laponite nanosilicates, into the hydrogel formulation to promote bone healing. These synthetic Laponite  
23  
24 SNs are anionic nanoplates with a diameter around 30 nm and a thickness of 1 nm. Upon degradation, the  
25  
26 released non-toxic byproducts, such as magnesium ions, lithium ions, and orthosilicic acid, have been  
27  
28 identified with various bioactivities.<sup>35-37</sup> Therefore, it has been reported that this type of SNs can promote  
29  
30 osteogenic differentiation of human mesenchymal stem cells (hMSCs) even without the presence of growth  
31  
32 factors.<sup>35-37</sup>

33  
34 By applying this multifunctional hydrogel coating on bone implants, it is expected that the resulting coated  
35  
36 implants could show enhanced adhesion due to the strong binding interactions between catechol motifs and  
37  
38 Ti surfaces, present potent antimicrobial activity due to the incorporation of AMP, enhanced cell adhesion  
39  
40 due to the existence of RGD motifs in the gelatin backbone, and improved osteogenesis because of the  
41  
42 presence of SNs. Compared to conventional growth factors (e.g. bone morphogenetic protein 2 or BMP-2),  
43  
44 SNs have much higher biostability and lower cost.<sup>37</sup> AMP HHC-36 has presented potent antimicrobial  
45  
46 activity with low resistance, along with no inhibition side effect on bone formation; these make HHC-36  
47  
48  
49  
50  
51  
52  
53  
54  
55  
56  
57  
58  
59  
60

1  
2 very attractive for implants where osteointegration is critical.<sup>8,10,11</sup> In this study, we expect that the  
3  
4 combination of SNs, HHC-36, and catechol-modified GelMA will lead to the easy production of a  
5  
6 multifunctional implant surface with unique antimicrobial, osteogenic, and adhesive properties. *In vitro*  
7  
8 physical characterization and adhesion tests were performed to validate the strong binding between the  
9  
10 hydrogel coating with Ti implant surface. In addition, the antimicrobial activity and cytotoxicity of the  
11  
12 coating hydrogel, as well as the induction of hMSCs towards osteogenic differentiation, were tested *in vitro*.  
13  
14  
15  
16

## 17 **2. Materials and Methods**

### 18 **2.1. Materials**

19  
20 Type-A gelatin from porcine skin (300 bloom), methacrylic anhydride (94%),  
21  
22 2-hydroxy-1-[4-(2-hydroxyethoxy)phenyl]-2-methyl-1-propanone (Irgacure 2959, 98%), bovine serum  
23  
24 albumin (BSA, 98%), dimethyl sulfoxide (DMSO, 99%), succinic anhydride (99%), triethylamine (99%),  
25  
26 2-(*N*-morpholino)ethanesulfonic acid hemisodium salt (MES, 98%), ammonium hydroxide (28%-30%),  
27  
28 acetic acid (99.7%), *N*-(3-dimethylaminopropyl)-*N'*-ethylcarbodiimide hydrochloride (EDC, 98%),  
29  
30 *N*-hydroxysuccinimide (NHS, 98%), dopamine hydrochloride (98%), hydrochloric acid (36.5%), Triton™  
31  
32 X-100 (BioXtra), deuterium oxide (D<sub>2</sub>O, 99.9% in D), sodium hydroxide (NaOH, 98%), β-glycerol  
33  
34 phosphate (99%), L-ascorbic acid (99%), Alizarin Red S (certified by the Biological Stain Commission), and  
35  
36 dexamethasone (97%) were purchased from Sigma-Aldrich (St. Louis, MO, USA). Type II collagenase was  
37  
38 purchased from Worthington Biochemical Cor. (Lakewood, NJ, USA). Paraformaldehyde (16% aqueous  
39  
40 solution) was obtained from EMS (Hatfield, PA, USA). AMP HHC-36 was purchased from CPC Scientific  
41  
42 (Sunnyvale, CA, USA).  
43  
44  
45  
46  
47  
48  
49  
50

51  
52 Fetal bovine serum (FBS), Live/dead® Viability/Cytotoxicity Kit, PrestoBlue Cell Viability Reagent, Alexa  
53  
54 Fluor 594-phalloidin, 4',6-diamidino-2-phenylindole (DAPI), alpha minimum essential medium (α-MEM),  
55  
56 phosphate buffered saline (PBS), 2-[4-(2-hydroxyethyl)piperazin-1-yl] ethane sulfonic acid (HEPES buffer,  
57  
58  
59  
60



1  
2 25 mM, pH 7.4), trypsin-ethylenediaminetetraacetic acid (trypsin-EDTA), L-glutamine, and antibiotics  
3  
4 (Penicillin/Streptomycin) were purchased from Thermo Fisher Scientific (Waltham, MA USA). hMSCs  
5  
6 (PT-2501) and Poietics MSCGM BulletKit were purchased from Lonza (Basel, Switzerland). *Pseudomonas*  
7  
8 *aeruginosa* (*P. aeruginosa*, ATCC H1001:luxCDABE), *Escherichia coli* (*E. coli*, ATCC 25292),  
9  
10 *Staphylococcus aureus* (*S. aureus*, ATCC 25293), *Staphylococcus epidermidis* (*S. epidermidis*, ATCC 12228)  
11  
12 bacteria, Basal Medium 2 (BM2), and Mueller Hinton Broth (MHB) were obtained from ATCC (Manassas,  
13  
14 VA, USA).  
15  
16  
17  
18  
19

## 20 2.2. Synthesis of GelMA-COOH

21  
22 GelMA with a high degree of functionalization (~90%) was prepared according to previously reported  
23  
24 procedure.<sup>34,38</sup> Purified GelMA (2.0 g) was then fully dissolved in 40 mL PBS at 50 °C with magnetic  
25  
26 stirring, followed by the addition of triethylamine (1.0 mL) and a solution of succinic anhydride (1.0 g)  
27  
28 dissolved in 20 mL dimethyl sulfoxide (DMSO). The resulting mixture was stirred overnight at 50 °C,  
29  
30 diluted with 100 mL PBS, neutralized by 0.1 M HCl, and dialyzed against deionized water using 3.5 kDa  
31  
32 cutoff dialysis tubing for one week at room temperature to remove the impurities. The solution was  
33  
34 lyophilized to generate GelMA-COOH as a white foam (typical yield: ~80%).  
35  
36  
37  
38  
39

## 40 2.3. Synthesis and characterization of GelMA-DOPA

41  
42 To conjugate with the catechol motifs, GelMA-COOH (1.0 g) was dissolved in 10 mL MES buffer (50 mM,  
43  
44 pH = 5). The solution was degassed by bubbling N<sub>2</sub> for 15 min, followed by the addition of EDC (0.20 g),  
45  
46 NHS (0.30 g), and dopamine hydrochloride (0.20 g). Under the protection of N<sub>2</sub>, the resulting mixture was  
47  
48 stirred overnight at 25 °C. The solution was dialyzed against 0.01 M HCl in deionized water using 3.5 kDa  
49  
50 cutoff dialysis tubing for 4 days, neutralized by 0.01 M NaOH, and lyophilized to generate GelMA-DOPA  
51  
52 polymer as a white foam (typical yield: ~70%). Proton nuclear magnetic resonance (<sup>1</sup>H NMR) spectrum was  
53  
54 used to confirm the successful conjugation of the catechol motifs to GelMA. The degree of catechol motif  
55  
56  
57  
58  
59  
60

1  
2 functionalization was determined using UV spectrophotometry.  
3

#### 4 2.3.1. $^1\text{H}$ NMR tests

5  
6  
7  $^1\text{H}$  NMR spectra of GelMA, GelMA-COOH, and GelMA-DOPA polymers were obtained in  $\text{D}_2\text{O}$  (99.9% D,  
8 Cambridge Isotope Laboratories, Inc, Tewksbury, MA, USA) at a concentration of 2% (w/v) using a Varian  
9 Mercury 300 MHz NMR spectrometer. All  $^1\text{H}$  NMR spectra were referenced to the peak of residual proton  
10 impurities in  $\text{D}_2\text{O}$  at  $\delta = 4.75$  ppm. The NMR data were processed using the ACDLABS 12.0 software  
11 (Academic Edition).  
12  
13  
14  
15  
16  
17  
18

#### 19 2.3.2. Determination of catechol content by UV spectrophotometry

20  
21 A series of dopamine hydrochloride solutions in deionized water were prepared with concentrations ranging  
22 from 0.05 to 0.5 mM as the standard solutions to obtain the working curve. The synthesized GelMA-DOPA  
23 polymer was dissolved in 50 mM MES buffer at 2.0 mg/mL to prepare the sample solutions. UV-Vis  
24 absorption spectra of the solutions were measured between 200 to 400 nm. Absorbance values at 280 nm  
25 were plotted against concentrations of dopamine hydrochloride solutions to set up the working curve.  
26  
27 Absorbance of the sample solution at 280 nm was compared to the working curve to calculate the content of  
28 catechol motifs.  
29  
30  
31  
32  
33  
34  
35  
36  
37  
38

#### 39 2.4. UV crosslinking and characterization of GelMA-DOPA hydrogels

40  
41 GelMA-DOPA polymer was dissolved in PBS at different concentrations (5-20% (w/v)). Irgacure 2959 was  
42 added to the solution at 0.5% (w/v) as the photoinitiator. Photocrosslinked GelMA-DOPA hydrogels were  
43 formed by pipetting certain amount of the prepolymer solution into the desired mold or on the surface of  
44 glass slides and exposing to  $6.9 \text{ mW/cm}^2$  UV light (360-480 nm) for 60 s. Composite hydrogels with the  
45 addition of SNs and/or AMP were fabricated similarly with solutions containing both the photoinitiator (0.5%  
46 (w/v)) and the additives at desired concentrations.  
47  
48  
49  
50  
51  
52  
53  
54  
55  
56

#### 57 2.4.1. Swelling analysis

1  
2 Swelling ratios of GelMA-DOPA hydrogels were evaluated at 37 °C in PBS following previously reported  
3 procedures.<sup>39</sup> To prepare GelMA-DOPA hydrogels for swelling ratio tests, 50 μL prepolymer solution was  
4 first transferred into a custom-made polydimethylsiloxane (PDMS) mold with a diameter of 8 mm and a  
5 depth of 1 mm. A glass coverslip was used to cover the mold before irradiation by UV light for 60 s.  
6  
7 Hydrogel samples (5-20% (w/v)) were removed from the mold and coverslip, soaked in PBS, and incubated  
8 at 37 °C for 24 h to reach the equilibrium swelling state. The swollen hydrogel samples were weighed,  
9 which were then lyophilized to record their dry weights. The swelling ratios of hydrogel samples of 5-20%  
10 (w/v) concentrations were then calculated as the ratio of mass increase after swelling to the mass of dried  
11 samples.  
12  
13  
14  
15  
16  
17  
18  
19  
20  
21  
22  
23

#### 24 2.4.2. *In vitro* degradation tests

25  
26 Hydrogel samples for degradation tests were prepared similarly as explained for swelling ratio  
27 measurements. The as-prepared samples were soaked in PBS at 37 °C for 24 h to reach the equilibrium  
28 swelling state and then were weighed to record their initial masses. The GelMA-DOPA hydrogel samples of  
29 5-20% (w/v) concentrations were kept in type II collagenase PBS solutions (2 U/mL) at 37 °C with mild  
30 shaking and the remaining masses were regularly recorded at different time points (days 7, 14, and 21) to  
31 track the degradation kinetics.  
32  
33  
34  
35  
36  
37  
38  
39  
40  
41

#### 42 2.5. Mechanical characterizations

##### 43 2.5.1. Compression tests

44  
45 Cylindrical crosslinked samples were prepared (10 mm in diameter, 2 mm in height) and incubated at 37 °C  
46 in PBS for 24 h. The GelMA-DOPA hydrogel samples of 5-20% (w/v) concentrations were then compressed  
47 at a rate of 1 mm/min using an Instron 5542 mechanical tester. Compressive moduli of the samples were  
48 determined as the slope in the linear region corresponding to 0–10% strain.  
49  
50  
51  
52  
53  
54  
55  
56

##### 57 2.5.2. Lap shear tests

1  
2 The adhesive properties of hydrogels were analyzed using an ASTM standard lap shear test (F2255-05) with  
3  
4 modifications. Briefly, 20  $\mu\text{L}$  of the prepolymer solution was applied to a glass slide pretreated with  
5  
6 3-(trimethoxysilyl)propyl methacrylate (TMSPMA). A Ti slide or a second TMSPMA-treated glass slide  
7  
8 was put into contact with the hydrogel to result in an overlapping (adhesive bonded) area of around  $2.0\text{ cm} \times$   
9  
10  $2.0\text{ cm}$ . After UV light irradiation for 60 s ( $6.9\text{ mW/cm}^2$ ), the samples were immersed in PBS for 2 hours  
11  
12 and then immediately strained under wet conditions until failure in lap shear setup using an Instron 5542  
13  
14 mechanical tester equipped with a 100-N load cell at a cross-head speed of 1.3 mm/min. To examine the  
15  
16 hydrogel residue on Ti substrates after breaking, a rhodamine dye was added to the prepolymer solution as a  
17  
18 fluorescent indicator.  
19  
20  
21  
22  
23

## 24 2.6. *In vitro* cell culture

25  
26 hMSCs were cultured in a 5%  $\text{CO}_2$  humidified incubator at 37  $^\circ\text{C}$  in normal growth media (Poietics  
27  
28 MSCGM BulletKit). Only cells before passage 5 were used for all the experiments. The osteoconductive  
29  
30 medium was supplemented with  $\beta$ -glycerol phosphate and L-ascorbic acid, and the osteoinductive medium  
31  
32 was supplemented with  $\beta$ -glycerol phosphate, ascorbic acid, and dexamethasone to induce osteogenic  
33  
34 differentiation of hMSCs. The cells were passaged approximately 1 time per week and the culture medium  
35  
36 was changed every 2 days. The cells were trypsinized, resuspended, and seeded on hydrogel-coated Ti slides  
37  
38 placed in a 24-well plate at a density of 50,000 cells per well.  
39  
40  
41  
42  
43  
44

### 45 2.6.1. Cell viability

46  
47 Cell viability was determined using a Live/Dead assay kit following the manufacturer's instructions. Briefly,  
48  
49 the cells were stained with calcein AM (0.5  $\mu\text{L/mL}$ ) and ethidium homodimer-1 (EthD-1, 2  $\mu\text{L/mL}$ ) in PBS  
50  
51 for live and dead cells, respectively. The cells were incubated at 37  $^\circ\text{C}$  for 20 min, and thoroughly washed  
52  
53 with PBS for three times. The stained cells were imaged using an inverted fluorescence microscope (Nikon  
54  
55 TE 2000-U, Nikon instruments Inc., USA). The numbers of live and dead cells were counted using the  
56  
57  
58  
59  
60

1  
2 ImageJ software from at least 3 images from different areas of 3 samples for each experimental condition.

3  
4 Cell viability was calculated as the number of live cells divided by the total cell number.

#### 5 6 7 2.6.2. Cell adhesion, proliferation, and spreading

8  
9 DAPI and Alexa Fluor 594-phalloidin were used to stain the cells for investigating the attachment and  
10 spreading of cells on the hydrogel surfaces. Cells seeded on different substrates were fixed in 4% (v/v)  
11 paraformaldehyde for 30 min, followed by treatment with a 0.1% (w/v) Triton X-100 solution in PBS for 20  
12 min to increase permeability, and with a 1% (w/v) BSA solution in PBS for 1 h to block non-specific binding  
13 sites. The cells were then incubated in a 1:40 dilution of Alexa Fluor 594-phalloidin in 0.1% (w/v) BSA for  
14 45 min to stain the actin cytoskeleton, and then incubated at 37 °C in a 0.1% (w/v) DAPI solution in PBS for  
15 10 min to stain the cell nuclei. After each staining step, the samples were carefully washed with PBS for  
16 three times before visualizing with the Nikon TE 2000-U microscope. ImageJ software was used to count  
17 the number of DAPI stained nuclei.  
18  
19

#### 20 21 22 2.7. PCR experiments

23  
24 PCR experiments were performed to quantify the expression of biomarkers related to osteogenesis. For  
25 quantitative PCR (qPCR) experiments, SYBR Green Real-Time PCR Master Mixes (Thermo Fisher  
26 Scientific) and primers obtained from Integrated DNA Technologies (IDT, Coralville, Iowa, USA) were used  
27 (see Table S1 in the Supporting Information).  
28  
29

#### 30 31 32 2.8. Alizarin Red S staining

33  
34 Cells were fixed with 10% formalin for 20 min and then thoroughly washed with PBS and DI water, before  
35 the addition of a 2% (w/v) solution of Alizarin Red S with pH = 4.2. After 10 min incubation at 37 °C, the  
36 samples were washed with DI water for microscope imaging. To quantify the coloration after staining, 10%  
37 (v/v) acetic acid was added to the cells and incubated overnight. After that, the resulting mixture was  
38 centrifuged for 15 min at 20000g and the supernatant was collected and neutralized with 10% (v/v)  
39  
40  
41  
42  
43  
44  
45  
46  
47  
48  
49  
50  
51  
52  
53  
54  
55  
56  
57  
58  
59  
60

1  
2 ammonium hydroxide. The absorption value at 405 nm of the solutions was recorded using a microplate  
3  
4 reader.  
5

## 6 7 2.9. Release profile of AMP HHC-36 8

9  
10 *In vitro* release profile of AMP loaded within 20% (w/v) GelMA-DOPA hydrogels was obtained by using  
11  
12 ultraviolet-visible (UV-Vis) spectroscopy. The absorptions at 280 nm, known as the characteristic absorption  
13  
14 peak for tryptophan residues, were recorded to monitor the concentration of released AMP in solutions. The  
15  
16 hydrogel specimens were prepared in triplicate by coating on a Ti substrate and then immersed in 1 mL of  
17  
18 PBS in a glass vial with rotation at 37 °C. At designed time points, 500 µL of the solution was removed from  
19  
20 the vial with fresh PBS replenished. Absorptions at 280 nm of the sample solutions were measured to  
21  
22 determine the cumulative release ratio of AMP. A series of standard solutions of AMP in the concentration  
23  
24 range of 1 to 128 µg/mL in deionized water were prepared to obtain the working curve. Quantification of  
25  
26 AMP concentration was then calculated based on the external standard curve method. The release  
27  
28 experiment was performed using GelMA-DOPA hydrogel samples without AMP loads as the blank control  
29  
30 to eliminate the possible influence from degraded hydrogel fragments.  
31  
32  
33  
34  
35  
36

## 37 2.10. Antimicrobial activity testing 38

39  
40 Antimicrobial activity of the AMP-loaded GelMA-DOPA hydrogels was tested against both Gram-positive  
41  
42 (*S. aureus* and *S. epidermidis*) and Gram-negative (*P. aeruginosa* and *E. coli*) bacteria in the mid-logarithmic  
43  
44 phase of growth. The bacterial suspensions were re-suspended using BM2 or MHB to reach a final cell  
45  
46 density of 10<sup>6</sup> colony-forming units (CFU)/mL. To perform the survival assay, 400 µL of the bacterial  
47  
48 suspensions were dropped onto three bare Ti plates, three GelMA-DOPA-coated Ti plates, and three  
49  
50 GelMA-DOPA-coated Ti plates loaded with AMP (1 mg/mL), respectively, followed by rinsing with distilled  
51  
52 water. After 4 h and 24 h incubation with *P. aeruginosa*, *E. coli*, *S. aureus*, and *S. epidermidis* bacterial  
53  
54 suspensions, samples were taken and inoculated on nutrient agar plates and incubated overnight at 37 °C.  
55  
56  
57  
58  
59  
60

1  
2 Bacterial survival rates were assessed by counting the number of CFUs. The antimicrobial activity of  
3  
4 hydrogel samples was also confirmed by scanning electron microscopy (SEM) imaging of samples  
5  
6 incubated with  $10^6$  CFU/mL of the selected bacteria overnight at 37 °C. SEM images were obtained using a  
7  
8 FEI/Philips XL30 FEG ESEM instrument (15 KV). The substrate without AMP-loaded GelMA-DOPA  
9  
10 coating layer was used as control.  
11

## 12 13 14 15 2.11. Statistical analysis

16  
17 For comparison, experimental data were processed using one-way ANOVA followed by Bonferroni's  
18  
19 post-hoc test (GraphPad Prism 5.02) software. Error bars represented the mean  $\pm$  standard deviation (SD) of  
20  
21 measurements (\* $p < 0.05$ , \*\* $p < 0.01$ , and \*\*\* $p < 0.001$ ).  
22  
23

## 24 25 3. Results and Discussion

### 26 27 3.1. Preparation of photocrosslinkable GelMA-DOPA

28  
29 Derived from partial hydrolysis of collagen, gelatin has been widely used in tissue engineering applications,  
30  
31 due to its biocompatibility, biodegradability, and low cost.<sup>20,40-44</sup> During the past few years, our group has  
32  
33 popularized the use of a photocrosslinkable gelatin derivative, GelMA, for various biomedical  
34  
35 applications.<sup>33,34,45-47</sup> Due to the existence of RGD sequences along the gelatin backbone, GelMA hydrogels  
36  
37 were found to support cell attachment and spreading.<sup>15,45</sup> To develop a sprayable coating material, adhesion  
38  
39 properties to both implant and tissue surfaces are critical. In recent years, inspired by natural adhesives  
40  
41 secreted by mussel species,<sup>22,24,28,48,49</sup> the mechanism of adhesion improvement by introduction of catechol  
42  
43 motifs has been widely applied to design adhesives with strong binding properties to diverse surfaces, in  
44  
45 particular wet surfaces.<sup>22</sup> Here, we propose to chemically conjugate GelMA polymer with dopamine (DOPA)  
46  
47 to introduce catechol motifs and synthesize GelMA-DOPA, which could combine the regenerative properties  
48  
49 of GelMA-based hydrogels with enhanced adhesion properties of the catechol motifs (Figure 1a).  
50  
51  
52  
53  
54  
55

56  
57 GelMA-DOPA was prepared from GelMA via a two-step procedure, as shown in Figure 1b. First, GelMA  
58  
59  
60

1  
2 was reacted with excess amount of succinic anhydride to fully convert all the remaining reactive amine  
3 groups to carboxylic groups. The resulting GelMA-COOH intermediate was then allowed to react with  
4  
5 dopamine hydrochloride via the EDC/NHS-mediated coupling reaction (Figure 1b). The resulting mixture  
6  
7 was then purified by dialysis against deionized water and finally lyophilized to obtain a white solid. Similar  
8  
9 to GelMA, the product GelMA-DOPA can also be crosslinked to form hydrogels by UV light exposure in the  
10  
11 presence of a photoinitiator, as shown in Figure 1c.

12  
13  
14  
15  
16  
17  $^1\text{H}$  NMR data of GelMA, GelMA-COOH, and GelMA-DOPA were obtained in  $\text{D}_2\text{O}$  to confirm the  
18  
19 successful conjugation of the catechol motifs. As shown in Figure 1d, in the  $^1\text{H}$  NMR spectrum of  
20  
21 GelMA-DOPA (blue line), additional peaks in the aromatic region appeared after the EDC/NHS coupling  
22  
23 reaction, which were not observed in the spectra of neither GelMA (black line) nor GelMA-COOH (red line).  
24  
25 These peaks are characteristic of the catechol motifs according to previous reports.<sup>50,51</sup> However,  
26  
27 comparison of the FT-IR spectra among GelMA, GelMA-COOH, and GelMA-DOPA did not result in  
28  
29 identifiable differences to reflect the introduction of the DOPA motifs (Figure S1). This is probably due to  
30  
31 the fact that the chemical modification did not add new functional groups that have characteristic IR  
32  
33 absorption peaks. In addition, there was a strong peak centered at 280 nm in the UV-Vis absorption spectrum  
34  
35 of GelMA-DOPA,<sup>52</sup> as shown in Figure 1e (blue line). By comparing with the spectra of dopamine  
36  
37 hydrochloride and the precursor GelMA-COOH, it is clear that this absorption peak appeared due to the  
38  
39 presence of the catechol motifs in GelMA-DOPA. To quantitatively determined the content of catechol  
40  
41 motifs, the absorption values at 280 nm ( $A_{280}$ ) of a series of dopamine hydrochloride solutions with different  
42  
43 concentrations ranging from 0 – 1 mmol/mL were measured and plotted to obtain a working curve. By  
44  
45 assuming that the conjugated catechol motifs have similar extinction coefficient with the free small  
46  
47 molecules, the content of catechol groups in GelMA-DOPA was determined as 0.5 mmol/g. This value  
48  
49 suggested roughly 5 catechol groups per 100 amino acid residues in the backbone.  
50  
51  
52  
53  
54  
55  
56  
57  
58  
59  
60



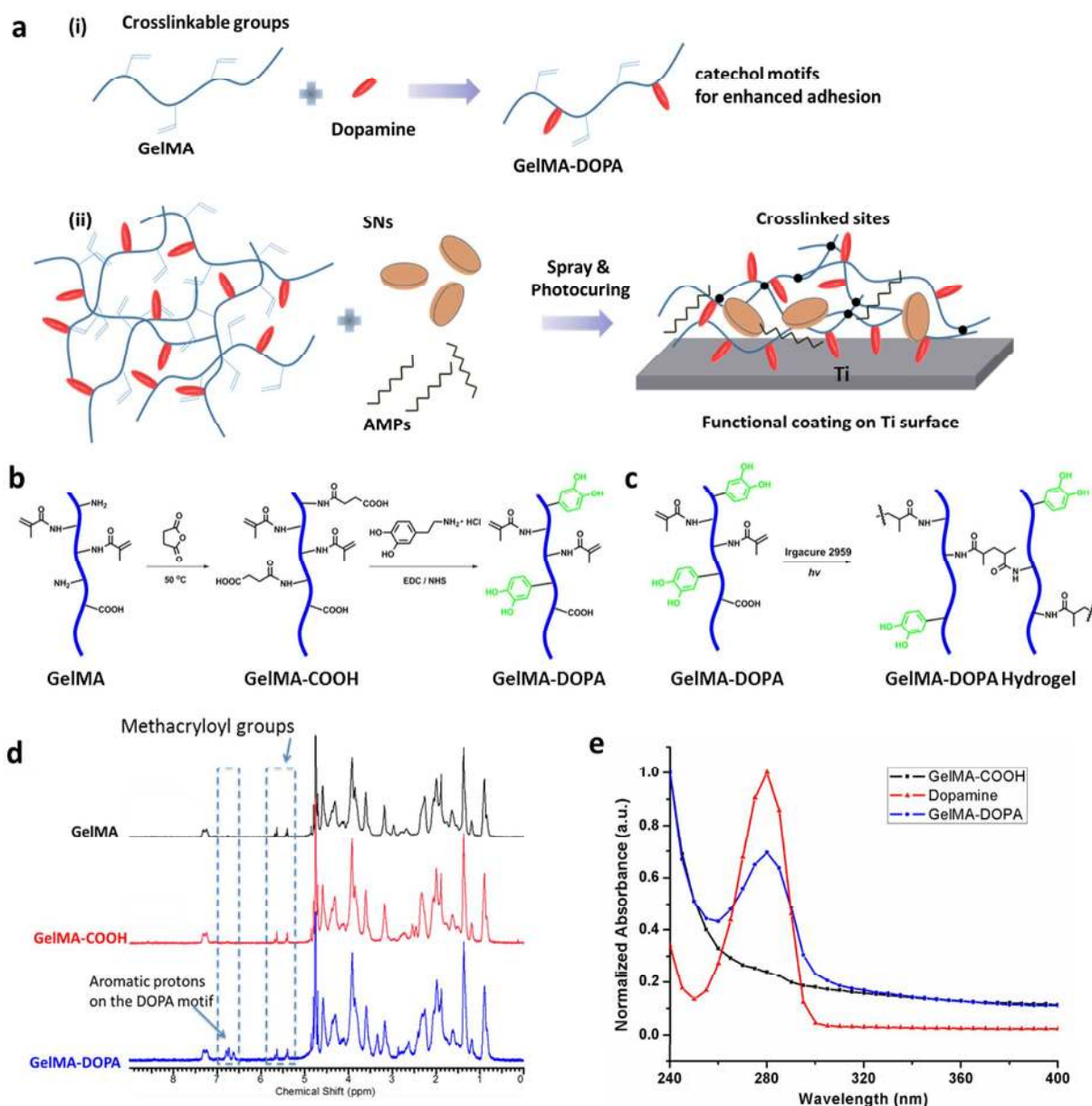


**Figure 1.** Synthesis and molecular characterization of the catechol-functionalized GelMA-DOPA hydrogel. **(a)** Schematic illustration for the formation of a highly adhesive, multifunctional hydrogel coating on Ti surfaces. **(i)** GelMA was modified with dopamine to introduce the catechol motifs that bind strongly to Ti. **(ii)** The hydrogel prepolymer solution was then mixed with the bioactive AMP and SNs, sprayed onto implant surface, and photo-cured *in situ* to form an antimicrobial and osteoinductive hydrogel coating layer. **(b)** Synthetic scheme of dopamine-containing GelMA (GelMA-DOPA). **(c)** Formation of crosslinked network with dangling dopamine motifs upon UV exposure in the presence of a photoinitiator. **(d)**  $^1\text{H}$  NMR spectra of GelMA, GelMA-COOH, and GelMA-DOPA. Comparison indicated that the appearance of additional resonance peaks in the aromatic region of GelMA-DOPA spectrum, which can be assigned to the DOPA motifs. **(e)** UV-Vis absorption spectra of GelMA-COOH, dopamine hydrochloride, and GelMA-DOPA. Appearance of the peak centered at 280 nm indicated successful conjugation of the DOPA motifs.

The catechol-modified photocrosslinkable GelMA-DOPA polymer was used to design sprayable antimicrobial and osteoinductive hydrogel coatings for implants. To introduce more functions, two

1  
2 additional components, namely AMP and SNs, were added to GelMA-DOPA macromers for improved  
3  
4 antimicrobial and osteoinductive properties. It has been shown that the release of AMP from the hydrogel  
5  
6 coating provides the antimicrobial activity,<sup>53,54</sup> and that exposure of hMSCs to the SNs is known to induce  
7  
8 osteogenic differentiation of hMSCs, as reported in previous publications.<sup>37,55,56</sup>  
9

### 10 11 3.2 Physical and adhesion characterizations of the engineered hydrogels 12 13

14 We characterized the physical properties of GelMA-DOPA hydrogels with different formulations in terms of  
15  
16 compressive modulus, swelling ratio, and degradation behavior. As shown in Figure 2a, the compression test  
17  
18 illustrated an expected positive correlation between GelMA-DOPA concentrations and the compressive  
19  
20 moduli of the resulting hydrogels, ranging from  $8.0 \pm 1.7$  kPa for 5% (w/v) GelMA-DOPA hydrogels to  $120$   
21  
22  $\pm 12$  kPa for 20% (w/v) hydrogels. The tunable compressive moduli of GelMA-DOPA hydrogels provide the  
23  
24 basis for fine tuning the properties of the hydrogel coating matrix, since it has been known that hydrogel  
25  
26 surfaces with different compressive moduli could affect the morphology, proliferation, and differentiation of  
27  
28 stem cells.<sup>57,58</sup>  
29  
30  
31  
32  
33

34 Addition of SNs (100  $\mu\text{g/mL}$ ) and AMPs (1.0  $\text{mg/mL}$ ) at the relevant concentrations did not show  
35  
36 significant influences on the compressive moduli of the 20% (w/v) GelMA-DOPA hydrogels (Figure 2b),  
37  
38 which could be attributed to the low loading concentrations. These concentrations were determined from  
39  
40 previous reports,<sup>10,37,56</sup> which have been shown as the optimized concentrations as functional additives. We  
41  
42 further analyzed the swelling ratios of GelMA-DOPA hydrogels fabricated from prepolymers of different  
43  
44 concentrations (Figure 2c), which indicated water absorption capacity. As expected, a reverse relationship  
45  
46 between swelling ratio and prepolymer concentration was identified, ranging from  $16.3 \pm 1.5$  for 5% (w/v)  
47  
48 GelMA-DOPA hydrogels to  $5.5 \pm 0.4$  for 20% (w/v) hydrogels. When mixed with different additives, the  
49  
50 swelling ratio of 20% (w/v) GelMA-DOPA hydrogels did not change significantly, which fell in a narrow  
51  
52 range of around 4.5 times (Figure 2d). The relatively low swelling ratio can limit the amount of water  
53  
54  
55  
56  
57  
58  
59  
60

penetration and the degree of volume change upon implantation, which is beneficial for applications as a hydrogel coating layer to metal implants.

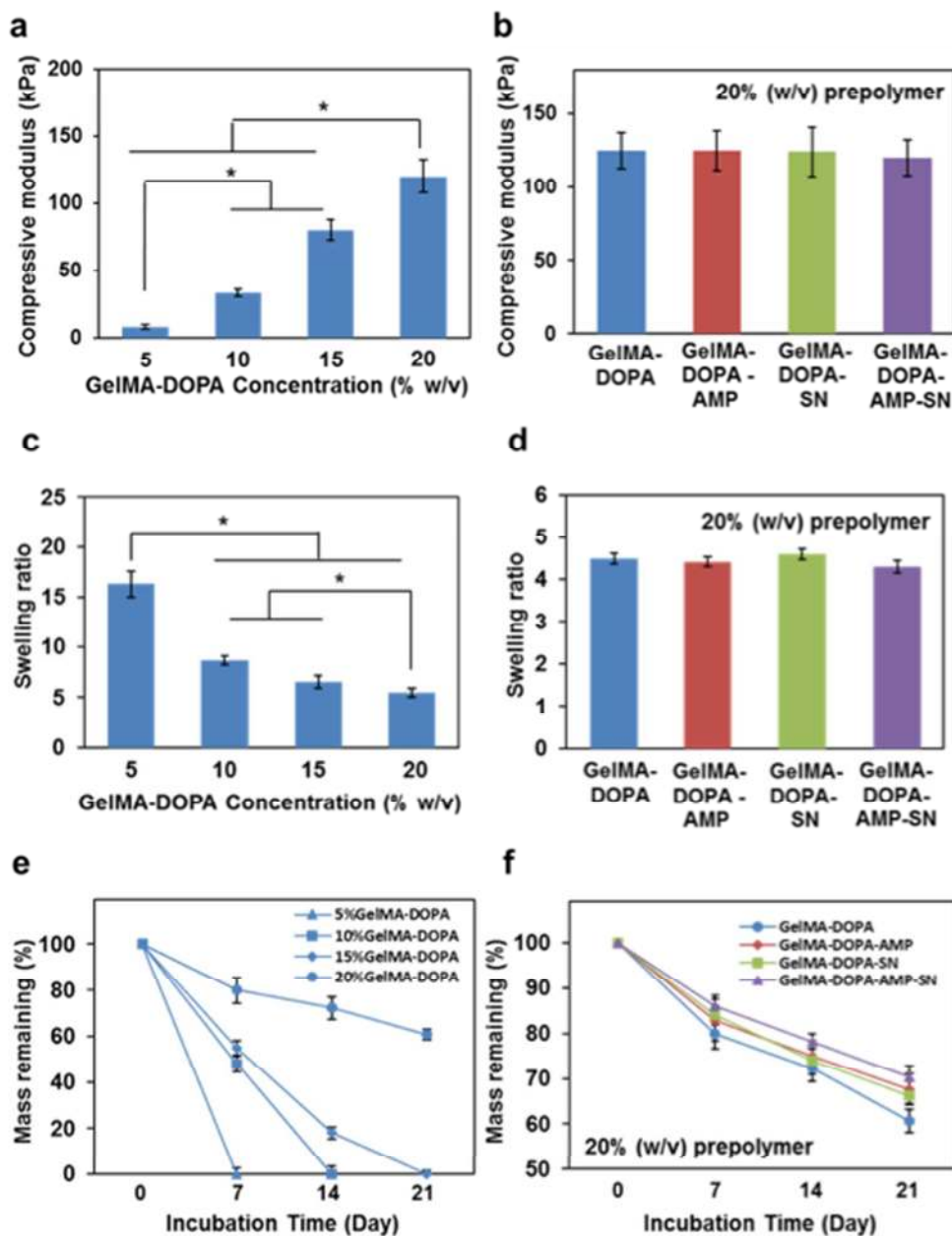


**Figure 2.** Physical characterizations of GelMA-DOPA hydrogels loaded with different additives. **(a)** Compressive moduli of GelMA-DOPA hydrogels at different prepolymer concentrations. **(b)** Compressive moduli of GelMA-DOPA hydrogels of 20% (w/v) prepolymer concentrations with AMP and/or SN additives. **(c)** Mass swelling of GelMA-DOPA hydrogels at different prepolymer concentrations. **(d)** Mass swelling of GelMA-DOPA hydrogels of 20% (w/v) prepolymer concentrations with AMP and/or SN additives. **(e)** *In vitro* degradation profiles of GelMA-DOPA hydrogels formed at different prepolymer concentrations. **(f)** Degradation profiles of different hydrogel compositions of 20% prepolymer concentration (\* $p < 0.05$ ).

1  
2 To evaluate the degradation kinetics, GelMA-DOPA hydrogel samples were incubated in PBS solutions with  
3  
4 collagenase (2 U/mL) at 37 °C and the remaining masses were monitored at different time points. As shown  
5  
6 in Figures 2e and 2f, the degradation rates were faster for hydrogels fabricated from lower hydrogel  
7  
8 concentrations. For 20% (w/v) GelMA-DOPA hydrogels, the remaining mass was 60-70% at day 21. In  
9  
10 contrast, GelMA-DOPA hydrogels made from 5% to 15% (w/v) prepolymer concentrations totally  
11  
12 disappeared within one to three weeks. To serve as the hydrogel coating layer for Ti implants, stability of  
13  
14 hydrogels up to several weeks or longer is an important parameter to ensure that the delivery of loaded  
15  
16 components will cover the short-term (several weeks) recovery range after surgery. From these results, we  
17  
18 selected the 20% (w/v) hydrogels to investigate the effects of bioactive component addition on the  
19  
20 degradation kinetics. As shown in Figure 2f, the addition of AMP and SNs to 20% (w/v) GelMA-DOPA  
21  
22 hydrogels did not demonstrate significant changes in degradation rates, suggesting possible controlled  
23  
24 release of bioactive loadings from the hydrogel for up to several weeks.  
25  
26  
27  
28  
29  
30  
31

32 Considering the working conditions of implants, achieving improved adhesion properties to Ti surfaces  
33  
34 under wet environments is critical to the success of a multifunctional hydrogel coating on Ti implants.  
35  
36 Therefore, we performed lap shear tests under swollen conditions of the hydrogel adhesive layer to  
37  
38 characterize the *in vitro* adhesion properties of modified GelMA-DOPA based on the modified ASTM  
39  
40 standard F2255-05 (Figure 3a). As shown in Figure 3b, we observed enhanced lap shear strengths along with  
41  
42 increasing GelMA-DOPA concentrations, which ranged from  $19.6 \pm 1.9$  kPa for 5% (w/v) GelMA-DOPA  
43  
44 hydrogels to  $60.7 \pm 8.9$  kPa for 20% (w/v) GelMA-DOPA hydrogels (Figures 3b), likely due to an increased  
45  
46 DOPA motif content at higher prepolymer concentrations. When compared to pristine GelMA and  
47  
48 GelMA-COOH hydrogels at the same 20% (w/v) concentration (Figure 3c), it was revealed that the adhesion  
49  
50 strengths of GelMA-DOPA hydrogels ( $60.7 \pm 8.9$  kPa) were significantly higher than those of GelMA or  
51  
52 GelMA-COOH hydrogels ( $15.2 \pm 3.0$  kPa and  $16.4 \pm 0.3$  kPa, respectively). The almost 4-fold increase in  
53  
54  
55  
56  
57  
58  
59  
60

1  
2 lap shear adhesion strength of GelMA-DOPA hydrogel under wet conditions could be attributed to the strong  
3  
4 binding interactions between the catechol motifs in GelMA-DOPA hydrogels, which largely improved  
5  
6 coating stability on Ti surfaces.<sup>23</sup>  
7  
8

9  
10 The lap shear tests provided quantitative data to reflect the adhesion increase due to the introduction of  
11  
12 catechol motifs to the hydrogel, but these values could not show the possibly different failure modes from  
13  
14 the samples. To further understand the failure mode of hydrogel adhesives in lap shear tests, we investigated  
15  
16 the surface morphology of the Ti substrates after adhesion failure. To qualitatively assess the amount of  
17  
18 hydrogel residue on Ti substrates after adhesion failure in the lap shear tests, we mixed a rhodamine dye  
19  
20 with the prepolymer solutions to serve as a fluorescent indicator. After the lap shear tests, we checked the Ti  
21  
22 substrates under fluorescence microscope. As shown in Figure 3di, the Ti surface coated with GelMA-DOPA  
23  
24 was found still covered with dye-doped hydrogels, as compared with those coated with GelMA or  
25  
26 GelMA-COOH. These results indicated that the failure mechanism of GelMA-DOPA hydrogel in lap shear  
27  
28 tests is a cohesive failure due to the relatively low mechanical stiffness of the hydrogel. On the contrast, for  
29  
30 GelMA or GelMA-COOH, the breaking of adhesion is via adhesive failure due to the poor adhesion  
31  
32 capability of the hydrogel layer to Ti surfaces. This comparison highlighted the feasibility of introducing  
33  
34 catechol motifs towards enhanced hydrogel-metal adhesion.<sup>31</sup>  
35  
36  
37  
38  
39  
40  
41  
42  
43  
44  
45  
46  
47  
48  
49  
50  
51  
52  
53  
54  
55  
56  
57  
58  
59  
60

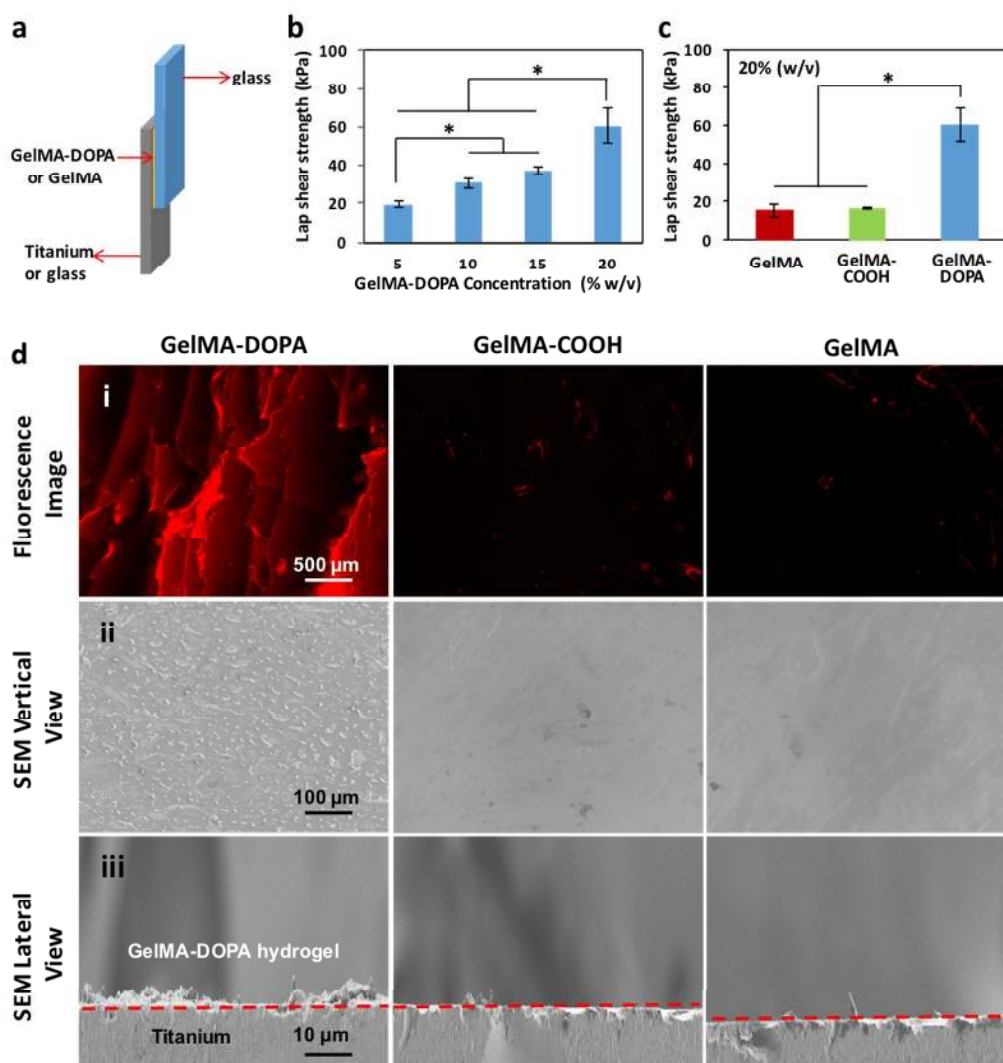


**Figure 3.** Adhesion properties of GelMA-DOPA hydrogels to titanium surface. **(a)** Schematic illustration of the experimental setup for testing the lap shear strength. **(b)** Lap shear strengths of GelMA-DOPA hydrogels of different prepolymer concentrations. **(c)** Comparison of lap shear strengths obtained from GelMA, GelMA-COOH, and GelMA-DOPA hydrogels of 20% (w/v) prepolymer concentration (\* $p < 0.05$ ). **(d)** Evaluation of titanium surfaces coated with different hydrogels after adhesion breaking in lap shear tests. (i) Representative fluorescent images of titanium surfaces coated with hydrogels mixed with a rhodamine dye. (ii-iii) Representative SEM images of titanium surfaces from (ii) vertical and (iii) lateral views.

We also used SEM to observe the morphological differences of the Ti substrates after lap shear tests coated with different hydrogels. As shown in Figure 3dii-iii, both vertical and lateral SEM images of the Ti substrates clearly showed the rough surface of GelMA-DOPA coated Ti plates with residue hydrogel coating due to the strong binding ability of this hydrogel. On the other hand, SEM images of GelMA and GelMA-COOH coated Ti substrates were relatively smooth with little hydrogel residue after lap shear tests.

1  
2 These results confirmed the different failure mechanisms of mussel-inspired GelMA-DOPA hydrogels and  
3  
4 pristine GelMA without catechol motifs. Since unmodified Ti substrates were used in these tests, the  
5  
6 increased adhesion with increasing GelMA-DOPA prepolymer concentrations were related to higher content  
7  
8 of catechol motifs, which provided stronger adhesion. This is different from other studies where surface  
9  
10 topology factors or surface energy differences of the Ti substrate play a role in improved adhesion  
11  
12 properties.<sup>59</sup> It is also suggested that the adhesion properties of catechol-containing hydrogels to Ti surfaces  
13  
14 might be further improved by increasing the cohesive strengths of the matrix hydrogels by known strategies  
15  
16 such as formulating hybrid hydrogels<sup>60</sup> or interpenetrated hydrogel networks.<sup>61</sup>

17  
18 From these results, it is revealed that in general swelling ratio is inversely correlated with GelMA-DOPA  
19  
20 prepolymer concentrations, while compressive modulus and lap shear strength are positively correlated with  
21  
22 prepolymer concentrations. Lower prepolymer concentrations typically resulted in lower crosslinking  
23  
24 density, and formation of hydrogels with lower mechanical properties. This is consistent with previous  
25  
26 studies on GelMA hydrogels where the modulus was reduced over 10-fold when the polymer concentration  
27  
28 decreased from 20% (w/v) to 5% (w/v).<sup>34</sup> For GelMA-DOPA samples, since the adhesion failure model is  
29  
30 cohesive failure (hydrogel breaking), lower mechanical strengths lead to lower lap shear strengths. Therefore,  
31  
32 the hydrogel with lower stiffness exhibited lower shear adhesion. Our results provide understandings  
33  
34 towards rationale design of hydrogel coatings with better performances.

### 35 36 37 3.3. Release profile of AMP from GelMA-DOPA hydrogels

38  
39 To incorporate antimicrobial activity to the sprayable and photocrosslinkable hydrogel coating material, a  
40  
41 broad-spectrum AMP HHC-36 was added in the prepolymer solution. The AMP HHC-36 has a sequence of  
42  
43 KRWWKWR, and has previously been loaded in calcium phosphate and vertically aligned titanium  
44  
45 oxide (TiO<sub>2</sub>) nanotube coatings on Ti surfaces to inhibit microbe growth.<sup>8-11</sup> It was demonstrated that these  
46  
47 positively charged short peptides could show high binding affinity towards the negatively charged bacteria  
48  
49  
50  
51  
52  
53  
54  
55  
56  
57  
58  
59  
60

1  
2 membrane through electrostatic interactions, thus promoting the targeting and antimicrobial capability.<sup>62</sup>  
3  
4 Importantly, the HHC-36 peptide showed no inhibition side effect on new bone formation, making it suitable  
5  
6 as additives for loading on Ti implants where osteointegration after implantation is important.<sup>8,10,11</sup> To  
7  
8 monitor the release profile of AMP HHC-36 from the crosslinked GelMA-DOPA hydrogel, 1 mg/mL AMP  
9  
10 was mixed with 20% (w/v) GelMA-DOPA prepolymer solutions containing 0.5% (w/v) photoinitiator.<sup>8,10</sup> To  
11  
12 achieve this, 20  $\mu$ L of the mixed solution was drop-coated on a glass slide and cured under 6.9 mW/cm<sup>2</sup> UV  
13  
14 light (360-480 nm) for 60 s to form the crosslinked hydrogel coating layer. The prepared samples were  
15  
16 incubated at 37 °C in PBS. The amount of AMP released from GelMA-DOPA hydrogel was determined by  
17  
18 measuring absorption at 280 nm (Figure S2a). Pristine GelMA-DOPA hydrogel samples with no AMP  
19  
20 loading were used as the blank control.  
21  
22  
23  
24  
25  
26

27 A burst release of AMP was observed to reach a cumulative release of 37% within the first 24 h post  
28  
29 incubation (Figure S2b). After that, a relatively steady release of AMP was observed for the next 20 days of  
30  
31 incubation, resulting in an increase of cumulative release to roughly 90%. Previous reports on the release of  
32  
33 AMP loaded in the calcium phosphate coating or TiO<sub>2</sub> nanotubes indicated much faster release kinetics,  
34  
35 which reached the maximum cumulative release amount within a few hours.<sup>8,10</sup> Steady sustained release of  
36  
37 the antimicrobial components could be achieved from a multilayered coating that combined three layers of  
38  
39 TiO<sub>2</sub> nanotubes, calcium phosphate, and a phospholipid film, but required a complicated fabrication  
40  
41 process.<sup>10</sup> Due to the lack of conjugation between AMP and the hydrogel matrix, we reason that the release  
42  
43 mechanism is diffusion controlled. Indeed, the release of AMP was accelerated with the presence of  
44  
45 collagenase (Figure S2b). The prolonged release of AMP from the GelMA-DOPA hydrogel coating layer is  
46  
47 believed as a critical criterion to achieve protection against implant-associated infections for the first few  
48  
49 weeks after surgery. Moreover, in cases that long-term delivery of AMP is required, this material design also  
50  
51 allows easy surface immobilization of AMPs through copolymerization during the photocrosslinking.  
52  
53  
54  
55  
56  
57  
58  
59  
60



1  
2 Therefore, we believe that our approach provides a suitable method for controlled release of AMP from Ti  
3  
4 implant surfaces.  
5

### 6 7 3.4. Antimicrobial activity of AMP-loaded GelMA-DOPA hydrogels 8

9  
10 The antimicrobial capability of the released AMP was first tested using the CFU assay. Two experimental  
11  
12 groups, GelMA-DOPA-AMP and GelMA-DOPA-AMP-SN, were tested with blank GelMA-DOPA  
13  
14 hydrogels as the control. Both representative Gram-positive bacteria (*S. aureus* and *S. epidermidis*) and  
15  
16 Gram-negative bacteria (*P. aeruginosa* and *E. coli*) were used to assess the antimicrobial activity of the  
17  
18 AMP-loaded hydrogels by the CFU counting method.<sup>10</sup> After 4 h and 24 h incubation, the CFU values were  
19  
20 measured and compared to the initial dose. For all the four different bacteria used in the test, the control  
21  
22 samples showed significant increases of CFU values during incubation as expected. In contrast, AMP-loaded  
23  
24 hydrogels demonstrated excellent antimicrobial activity since significant reduction (several orders of  
25  
26 magnitude) in CFUs was observed at 4 h and complete elimination of bacteria at 24 h (Figure 4, a-d). The  
27  
28 bactericidal effect was most profound against *S. epidermidis*, which showed the least CFU value after 4 h.  
29  
30 Moreover, the antimicrobial activity was not significantly influenced by the addition of SNs. Considering  
31  
32 the high initial numbers of bacteria ( $10^6 \sim 10^8$  CFU/mL), it is suggested that the loading of AMP in the  
33  
34 GelMA-DOPA hydrogel coating will be efficient in clinical circumstances, where the actual numbers of  
35  
36 bacteria encountered could be much lower.<sup>6</sup>  
37  
38  
39  
40  
41  
42  
43  
44

45 The antimicrobial activity was also evaluated by staining the bacteria using a Live/Dead assay. Four  
46  
47 different bacteria were seeded on the surface of hydrogel coatings and cultured for 24 h before staining.  
48  
49 Viability of the bacteria was monitored by measuring their membrane integrity. The green-fluorescent  
50  
51 nucleic acid dye is able to penetrate the cell membrane of both healthy and dead bacteria cells, while the  
52  
53 red-fluorescent propidium iodide dye penetrates only damaged membranes and quenches the green  
54  
55 fluorescence in dead cells.<sup>63</sup> As a result, this staining can provide direct, visualized identification and  
56  
57  
58  
59  
60

1  
2 differentiation between living and dead bacteria cells. As shown in Figure 4e, bacteria cultured with  
3  
4 GelMA-DOPA-AMP-SN hydrogels were found with very low viability after 24 h, in contrast with the  
5  
6 results from the GelMA-DOPA-SN formulation, which showed high cell viability for all four species of  
7  
8 bacteria. Similarly, the assay results for bacteria cultured on GelMA-DOPA-AMP and GelMA-DOPA  
9  
10 hydrogels also showed low viability and high viability, respectively (Figure S3a). Therefore, the significant  
11  
12 changes in bacteria viability was thus attributed to the release of AMP from the hydrogels.  
13  
14  
15

16  
17 Inhibition of biofilm formation is also a critical requirement to prevent implant-associated infections, since  
18  
19 bacteria attached to biofilms demonstrate enhanced resistance to antibiotics.<sup>4</sup> SEM images of the control  
20  
21 GelMA-DOPA-SN (Figure 4f, top panels) and GelMA-DOPA (Figure S3b, top panels) hydrogel surfaces  
22  
23 with seeded bacteria showed that the bacteria could adhere to the surface and form cell aggregates with  
24  
25 different morphologies after 48 h of incubation. Under similar conditions, however, only very few bacteria  
26  
27 were able to adhere to the GelMA-DOPA-AMP-SN (Figure 4f, bottom panels) and GelMA-DOPA-AMP  
28  
29 (Figure S3b, bottom panels) hydrogel surfaces, thus preventing biofilm formation over the surface. We  
30  
31 believe that the ability of AMP-loading GelMA-DOPA hydrogels to prevent biofilm formation is an  
32  
33 important aspect in clinical applications, where the removal of biofilm after its buildup is almost  
34  
35 impossible.<sup>64</sup> From the results of controlled release tests of AMP from the hydrogel coating and the  
36  
37 antimicrobial activity tests, it was confirmed that the AMP-loaded GelMA-DOPA hydrogels were able to  
38  
39 reduce bacterial growth and accumulation on the Ti implants, which is promising to address  
40  
41 infection-associated implant failures.  
42  
43  
44  
45  
46  
47  
48  
49  
50  
51  
52  
53  
54  
55  
56  
57  
58  
59  
60

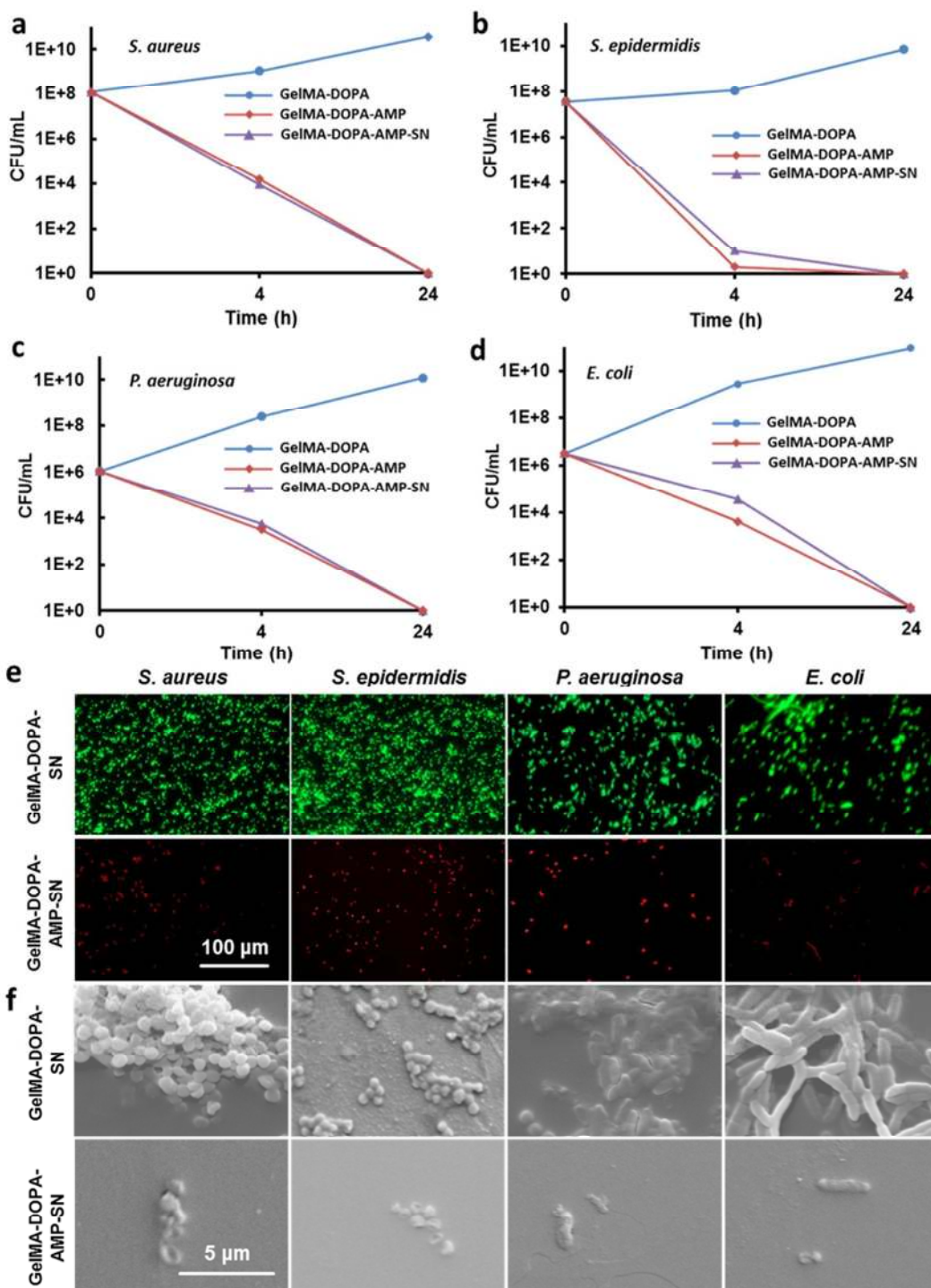


**Figure 4.** Antimicrobial activity of GelMA-DOPA hydrogels at 20% (w/v) prepolymer concentration with AMP and/or SN additives. **(a-d)** Bacteria colony count experiments against different bacteria, **(a)** *S. aureus*, **(b)** *S. epidermidis*, **(c)** *P. aeruginosa*, and **(d)** *E. coli*, seeded on different hydrogel formulations at 20% (w/v) concentration. Changes in CFU at 4 and 24 hours after incubation were taken as the measure of antimicrobial ability. Error bars in **(a-d)** are too small to present proportionally in the panels. **(e)** AMP released from GelMA-DOPA-AMP-SN samples demonstrated efficient antimicrobial ability to kill the tested bacteria, *S. aureus*, *S. epidermidis*, *P. aeruginosa*, and *E. coli*. Compared to GelMA-DOPA-SN samples without AMP loading, no live bacteria were observed on the GelMA-DOPA-AMP-SN samples after 24 h culture (green: live bacteria; red: dead bacteria; scale bar: 100  $\mu\text{m}$ ). **(f)** SEM images showing surfaces of GelMA-DOPA-SN and GelMA-DOPA-AMP-SN hydrogels incubated overnight with *S. aureus*, *S. epidermidis*, *P. aeruginosa*, and *E. coli*. Very few bacteria were observed on the AMP-loaded samples (scale

1 bar: 5  $\mu\text{m}$ ).

### 2 3 4 3.5. Cytotoxicity tests of GelMA-DOPA hydrogels

5  
6  
7 Cytotoxicity of the implant coating hydrogels was evaluated by 2D culture of hMSCs on hydrogel surfaces  
8  
9 with different formulations. Since the hydrogel coating formulation is based on a gelatin derivative, it is  
10  
11 expected that cell could adhere to the hydrogel coating surface and show spreading morphology due to the  
12  
13 existence of cell-adhesive motifs in the gelatin backbone.<sup>34,45,65</sup> The cells were seeded on the hydrogel  
14  
15 surfaces and cultured for 7 days. Cell viability was examined by the Live/Dead staining at days 1, 3, and 7  
16  
17 of culture. As shown in Figures 5a, 5c, and S4a, in general high viability (>90%) of the cells was observed  
18  
19 for all the experimental conditions, suggesting that this implant coating hydrogel was cytocompatible.  
20  
21 Moreover, the addition of AMP and SNs in the hydrogel at the doping concentrations did not reduce the high  
22  
23 cytocompatibility of the GelMA-DOPA based hydrogels, which is consistent with previous results.<sup>9,10,37,56</sup>

24  
25 The ability of the hydrogel surface to support cell spreading was validated by the staining of f-actin  
26  
27 filaments and nuclei of the cells (Figures 5b and S4b). In addition, quantification of the number of cell  
28  
29 nuclei in a unit surface area (Figure 5d) indicated that hMSCs seeded on the hydrogel surfaces were able to  
30  
31 proliferate along with increasing culture time. From counting the nuclei per unit area, the cell density of  
32  
33 hMSCs seeded on various GelMA-DOPA hydrogels increased almost 5-fold at day 7 compared with that at  
34  
35 day 1. These results confirmed that the presence of cell-binding motifs by using gelatin-based materials  
36  
37 could support cell spreading and cellular growth *in vitro*.<sup>34</sup>

38  
39 We also used the Prestoblue assay to monitor the metabolic activity of the seeded cells. The corrected  
40  
41 absorbance difference of the assay solution between 570 nm and 600 nm after culturing with cells for 2 h  
42  
43 was an indicator of the total metabolic activity of cells. As shown in Figure 5e, from day 1 to day 7, over  
44  
45 3-fold increase in absorbance difference was detected, reinforcing the conclusion that the hydrogel  
46  
47 formulations were not cytotoxic to hMSCs in *in vitro* cell culture.  
48  
49  
50  
51  
52  
53  
54  
55  
56  
57  
58  
59  
60

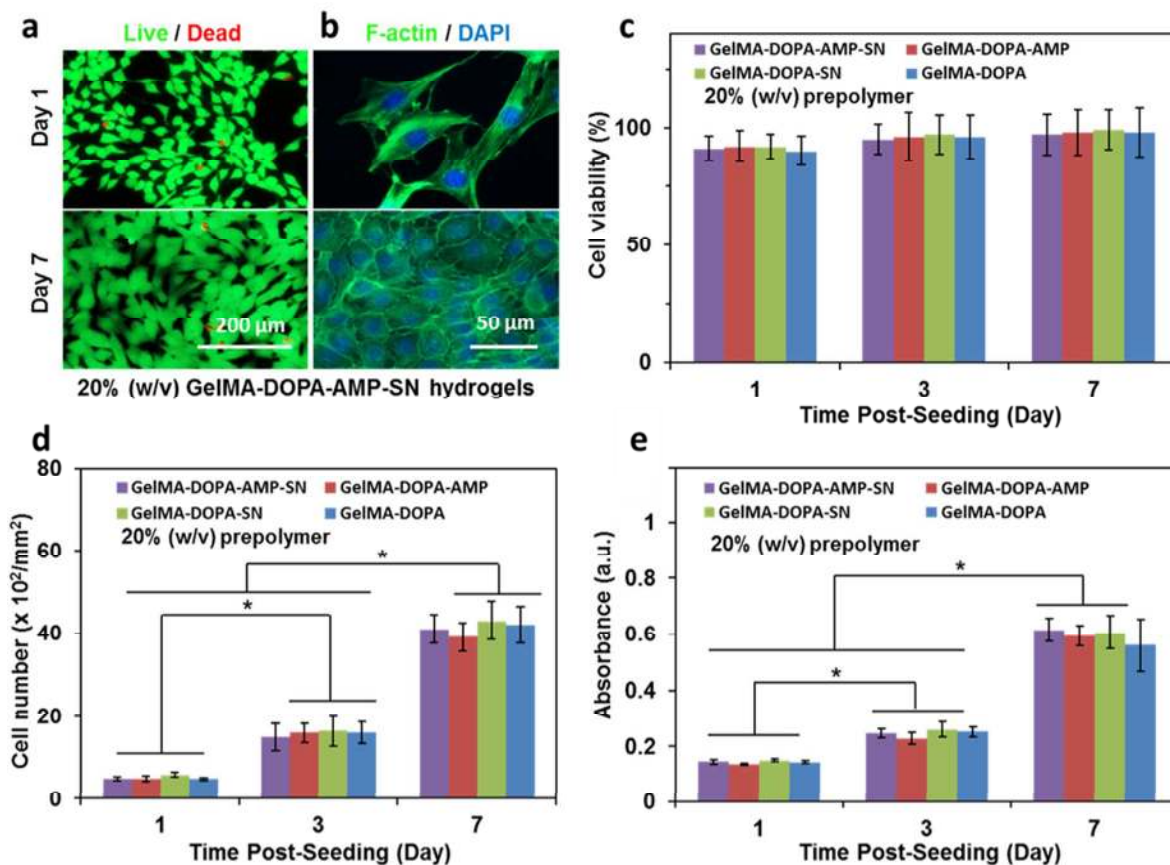


**Figure 5.** *In vitro* cytotoxicity of different hydrogel formulations at 20% (w/v) prepolymer concentration. **(a)** Representative Live/Dead staining images of hMSCs seeded on the surface of GelMA-DOPA-AMP-SN hydrogels on days 1 and 7 (scale bar: 200  $\mu\text{m}$ ). **(b)** Representative microscopic images of hMSCs seeded on the surface of GelMA-DOPA-AMP-SN hydrogels with staining for f-actin/cell nuclei on days 1 and 7 (scale bar: 50  $\mu\text{m}$ ). **(c)** Quantification of cell viabilities at 1, 3, and 7 days after cell seeding on different hydrogel surfaces. **(d)** Quantification of cell densities measured as the number of DAPI-stained nuclei per unit area at 1, 3, and 7 days after cell seeding on different hydrogel surfaces. **(e)** Corrected absorbance difference between 570 nm and 600 nm obtained from the Prestoblu assay at 1, 3, and 7 days after cell culture (\* $p < 0.05$ ).

### 3.6. Enhanced Osteogenesis of hMSCs

It has been reported that the SNs could induce osteogenic differentiation of stem cells including hMSCs even in the absence of any external osteoinductive factors.<sup>37,56</sup> As a result, when SNs are loaded in the spray formulation for implants, it is expected that the effects of osteogenesis induction could be used for improved integration with the surrounding tissues and enhanced new bone formation.<sup>7,15,66,67</sup> To validate this assumption, hMSCs seeded on different hydrogel surfaces were cultured in an osteogenic medium (100 nM dexamethasone, 10 mM  $\beta$ -glycerol phosphate, and 50  $\mu\text{g/mL}$  ascorbic acid). The expressions of several

representative osteogenic biomarkers were monitored using quantitative reverse transcriptase polymerase chain reaction (qPCR), such as the early osteogenic marker alkaline phosphatase (ALP), osteo-related proteins osteocalcin (OCN) and osteopontin (OPN), and Runt-related transcription factor 2 (RUNX2), which is a member of the RUNX transcription factor family and expressed in mineralized tissues.<sup>68,69</sup> Upregulation of these biomarkers is correlated with enhanced osteogenic differentiation of hMSCs. As shown in Figure 6, qPCR results suggested that when loaded with SNs, significantly enhanced expressions of ALP, OCN, OPN, and RUNX2 were observed at day 28. Moreover, the levels of protein expression did not significantly differ by introduction of AMP in the hydrogels, which is consistent with previous studies on AMP, making it suitable for the design of multifunctional implant coating hydrogel.<sup>8</sup>

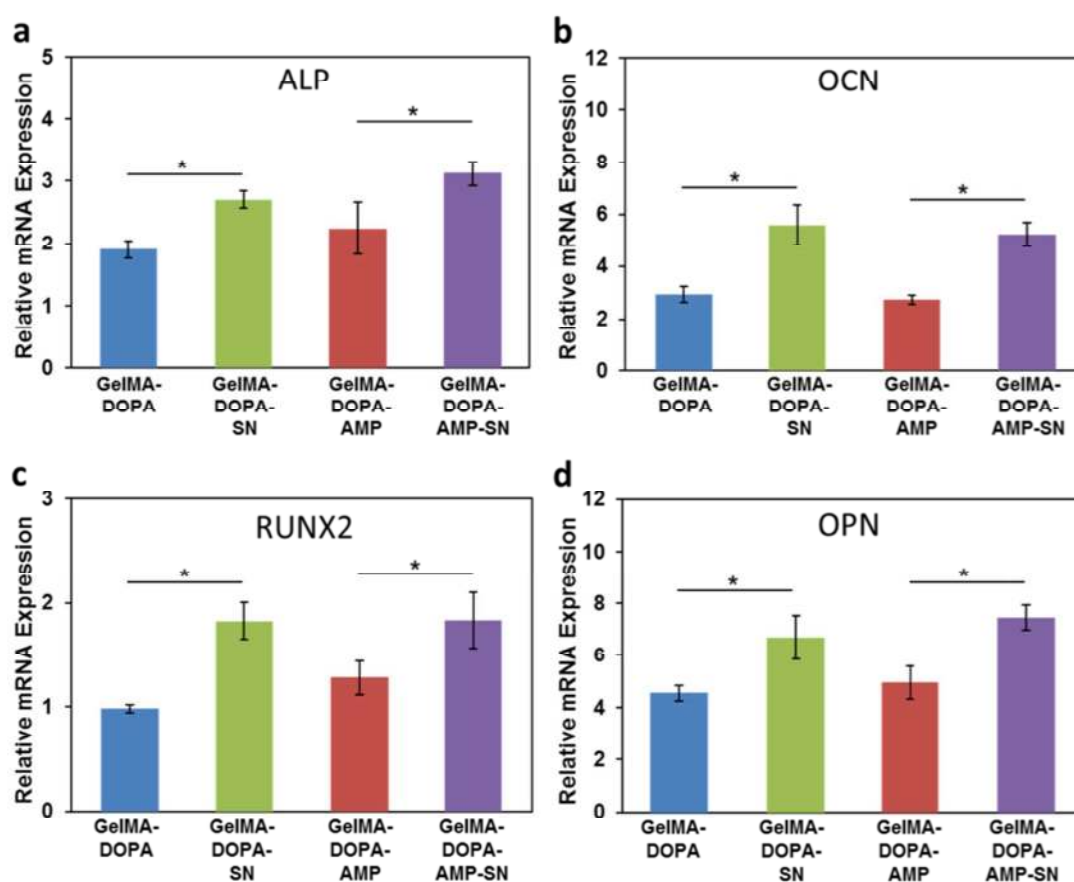


**Figure 6.** Effects of GelMA-DOPA hydrogels loaded with AMP and/or SN additives at 20% (w/v) prepolymer concentration on osteogenesis of hMSCs. (a-d) Enhanced osteogenesis was measured by qPCR quantification of relative mRNA expressions of osteogenic biomarkers: (a) ALP; (b) OCN; (c) OPN; and (d) RUNX2 at day 28 after incubation (\*p < 0.05).



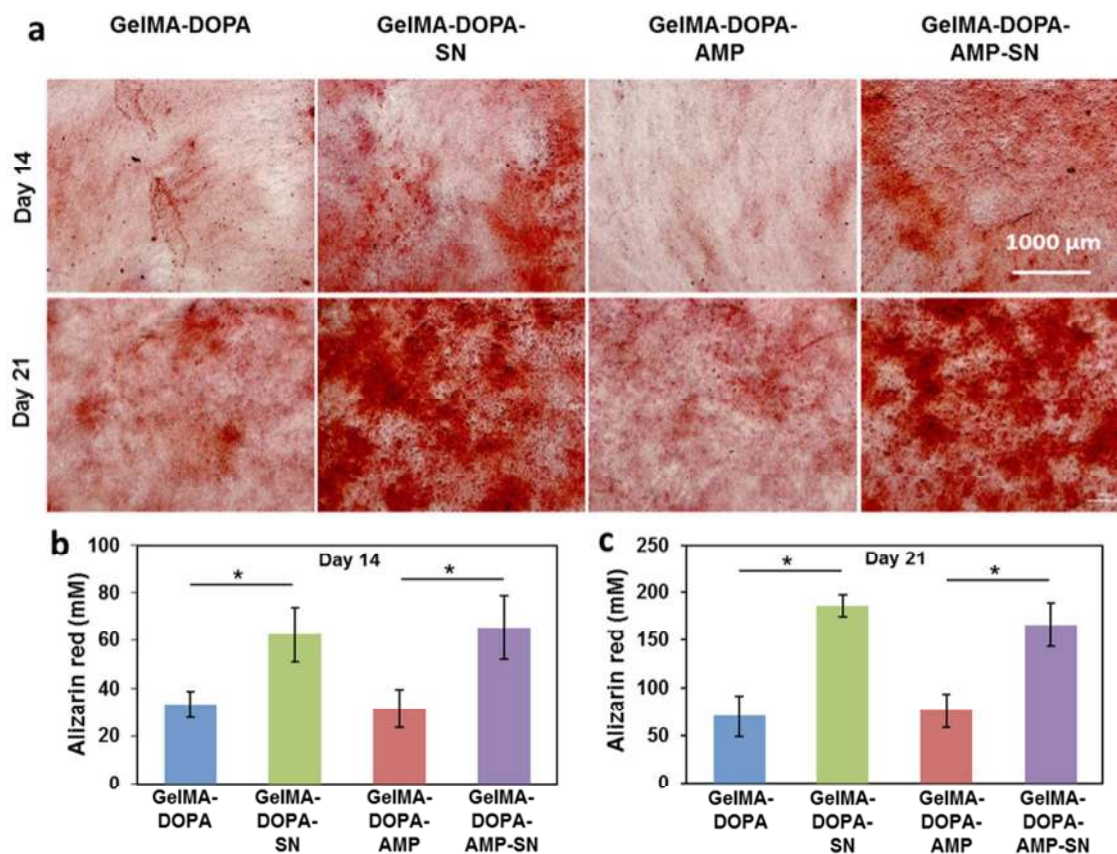


**Figure 7.** Effects of GelMA-DOPA hydrogels loaded with AMP and/or SN additives at 20% (w/v) prepolymer concentration on mineralized extracellular matrix production. **(a)** Quantitative analyses of mineralized extracellular matrix production in hMSCs were measured by the Alizarin Red S staining on days 14 and 21 of culture. **(b-c)** Quantification of the amount of Alizarin Red stain on **(b)** day 14 and **(c)** day 21 (\* $p < 0.05$ ).

The degree of mineralization of hMSCs cultured on hydrogel surfaces was analyzed by using the Alizarin Red S staining for the inorganic calcium deposition,<sup>37</sup> which is a characteristic indicator of the formation of bone-like structures as a result of osteogenic differentiation (Figure 7a). Compared to hydrogels without SN loadings, hMSCs cultured in the presence of SNs showed significantly enhanced production of extracellular matrix mineralization on both days 14 and 21 (Figures 7b and 7c). The increased mineralization was attributed to the bioactivity of SNs to promote osteogenic differentiation of hMSCs, which confirmed that when loaded in GelMA-DOPA hydrogels, the slow release of SNs can still induce mineral deposition of hMSCs *in vitro*.<sup>56</sup> These *in vitro* results indicated potential effects to promote osteointegration when implanted *in vivo*.<sup>1,18,70</sup>

#### 4. Conclusion.

In this study, we reported the design and evaluation of a mussel-inspired multifunctional coating hydrogel for implants to prevent infection and to promote osteogenesis of hMSCs. First, GelMA-DOPA was prepared by chemically conjugating catechol motifs to GelMA via the EDC/NHS chemistry to improve the adhesion of the hydrogel coating to Ti surfaces. After spray coating onto the implant surface, photocrosslinking was used to readily form the hydrogel coating. Enhanced adhesion of the hydrogel to Ti surfaces was observed as a result of the catechol motifs. Moreover, two additional active components, AMP HHC-36 and SNs, were loaded into the prepolymer solution to introduce the antimicrobial activity and the ability to induce osteogenesis. Prolonged release of AMP from the hydrogel was monitored to last for 21 days, which efficiently killed four different species of representative bacteria and thus prevented the formation of biofilms on the surfaces. In addition, the hydrogel formulations were found compatible to hMSCs and able to support cell adhesion, spreading, and proliferation in 2D culture models. Importantly, hMSCs cultured with SN-loading hydrogels demonstrated enhanced osteogenic differentiation, as confirmed by upregulated expressions of several osteo-related biomarkers revealed by qPCR and increased extracellular matrix mineralization revealed by the Alizarin Red S staining. These *in vitro* results suggested that this GelMA-DOPA based implant spray can provide a promising alternative method to design multifunctional hydrogel coating for Ti implants, including supporting cell adhesion, spreading and growth, preventing implant-associated infections, and enhancing implant integration with surrounding tissues by promoting osteogenesis of stem cells.

#### Conflict of interest.

The authors declare no conflict of interests in this work.

**Supporting Information.** The Supporting Information is available free of charge on the ACS Publications website.



1  
2 FT-IR spectra of GelMA, GelMA-COOH, and GelMA-DOPA (Figure S1), Release of AMP (Figure S2),  
3  
4 antimicrobial activity characterization (Figure S3), in vitro cytotoxicity and cellular evaluation (Figure S4),  
5  
6  
7 and primer sequences for qPCR experiments (Table S1) (PDF)  
8  
9

### 10 **Acknowledgement.**

11  
12 This paper is sponsored by the Institute for Soldier Nanotechnology, National Institutes of Health  
13  
14 (HL092836, EB02597, AR057837, HL099073), the National Science Foundation (DMR0847287), the  
15  
16 Office of Naval Research Young Investigator award, ONR PECASE Award. Y.S.Z. acknowledges the  
17  
18 National Cancer Institute of the National Institutes of Health K99/R00 Pathway to Independence Award  
19  
20  
21 (1K99CA201603-01A1).  
22  
23  
24  
25  
26  
27  
28  
29  
30  
31  
32  
33  
34  
35  
36  
37  
38  
39  
40  
41  
42  
43  
44  
45  
46  
47  
48  
49  
50  
51  
52  
53  
54  
55  
56  
57  
58  
59  
60

**References.**

- (1) Castellani, C.; Lindtner, R. A.; Hausbrandt, P.; Tschegg, E.; Stanzl-Tschegg, S. E.; Zanoni, G.; Beck, S.; Weinberg, A.-M. Bone-implant interface strength and osseointegration: Biodegradable magnesium alloy versus standard titanium control. *Acta Biomater.* **2011**, *7*, 432-440.
- (2) Cui, C.; Hu, B.; Zhao, L.; Liu, S. Titanium alloy production technology, market prospects and industry development. *Mater. Des.* **2011**, *32*, 1684-1691.
- (3) Veiga, C.; Davim, J.; Loureiro, A. Properties and applications of titanium alloys: a brief review. *Rev. Adv. Mater. Sci* **2012**, *32*, 133-148.
- (4) Arciola, C. R.; Campoccia, D.; Speziale, P.; Montanaro, L.; Costerton, J. W. Biofilm formation in Staphylococcus implant infections. A review of molecular mechanisms and implications for biofilm-resistant materials. *Biomaterials* **2012**, *33*, 5967-5982.
- (5) Zaat, S.; Broekhuizen, C.; Riool, M. Host tissue as a niche for biomaterial-associated infection. *Future Microbiol.* **2010**, *5*, 1149-1151.
- (6) Zhao, L.; Wang, H.; Huo, K.; Cui, L.; Zhang, W.; Ni, H.; Zhang, Y.; Wu, Z.; Chu, P. K. Antibacterial nano-structured titania coating incorporated with silver nanoparticles. *Biomaterials* **2011**, *32*, 5706-5716.
- (7) Cheng, H.; Xiong, W.; Fang, Z.; Guan, H.; Wu, W.; Li, Y.; Zhang, Y.; Alvarez, M. M.; Gao, B.; Huo, K. Strontium (Sr) and silver (Ag) loaded nanotubular structures with combined osteoinductive and antimicrobial activities. *Acta Biomater.* **2016**, *31*, 388-400.
- (8) Kazemzadeh-Narbat, M.; Kindrachuk, J.; Duan, K.; Jenssen, H.; Hancock, R. E.; Wang, R. Antimicrobial peptides on calcium phosphate-coated titanium for the prevention of implant-associated infections. *Biomaterials* **2010**, *31*, 9519-9526.
- (9) Ma, M.; Kazemzadeh-Narbat, M.; Hui, Y.; Lu, S.; Ding, C.; Chen, D. D.; Hancock, R. E.; Wang, R. Local delivery of antimicrobial peptides using self-organized TiO<sub>2</sub> nanotube arrays for peri-implant infections. *J. Biomed. Mater. Res. A* **2012**, *100*, 278-285.
- (10) Kazemzadeh-Narbat, M.; Lai, B. F.; Ding, C.; Kizhakkedathu, J. N.; Hancock, R. E.; Wang, R. Multilayered coating on titanium for controlled release of antimicrobial peptides for the prevention of implant-associated infections. *Biomaterials* **2013**, *34*, 5969-5977.
- (11) Kazemzadeh-Narbat, M.; Wang, Q.; Hancock, R. E.; Wang, R. Antimicrobial peptide delivery from trabecular bone grafts. *J. Biomater. Tissue Eng.* **2014**, *4*, 967-972.
- (12) Muszanska, A. K.; Busscher, H. J.; Herrmann, A.; van der Mei, H. C.; Norde, W. Pluronic-lysozyme conjugates as anti-adhesive and antibacterial bifunctional polymers for surface coating. *Biomaterials* **2011**, *32*, 6333-6341.
- (13) Zahran, M.; Ahmed, H. B.; El-Rafie, M. Surface modification of cotton fabrics for antibacterial application by coating with AgNPs-alginate composite. *Carbohydr. Polym.* **2014**, *108*, 145-152.
- (14) Shah, N. J.; Hyder, M. N.; Moskowitz, J. S.; Quadir, M. A.; Morton, S. W.; Seeherman, H. J.; Padera, R. F.; Spector, M.; Hammond, P. T. Surface-Mediated Bone Tissue Morphogenesis from Tunable Nanolayered Implant Coatings. *Sci. Transl. Med.* **2013**, *5*, 191ra183.
- (15) Chien, C.-Y.; Tsai, W.-B. Poly(dopamine)-Assisted Immobilization of Arg-Gly-Asp Peptides, Hydroxyapatite, and Bone Morphogenic Protein-2 on Titanium to Improve the Osteogenesis of Bone Marrow Stem Cells. *ACS Appl. Mater. Interfaces* **2013**, *5*, 6975-6983.
- (16) Nguyen, A. H.; McKinney, J.; Miller, T.; Bongiorno, T.; McDevitt, T. C. Gelatin methacrylate microspheres for controlled growth factor release. *Acta Biomater.* **2015**, *13*, 101-110.
- (17) Tsai, W.-B.; Chen, R. P.-Y.; Wei, K.-L.; Tan, S.-F.; Lai, J.-Y. Modulation of RGD-Functionalized Polyelectrolyte Multilayer Membranes for Promoting Osteoblast Function. *J. Biomater. Sci. Polym. Ed.* **2010**, *21*, 377-394.
- (18) Tang, W.; Policastro, G. M.; Hua, G.; Guo, K.; Zhou, J.; Wesdemiotis, C.; Doll, G. L.; Becker, M. L. Bioactive Surface Modification of Metal Oxides via Catechol-Bearing Modular Peptides: Multivalent-Binding, Surface Retention, and Peptide Bioactivity. *J. Am. Chem. Soc.* **2014**, *136*, 16357-16367.
- (19) Meng, Y.; Li, X.; Li, Z.; Liu, C.; Zhao, J.; Wang, J.; Liu, Y.; Yuan, X.; Cui, Z.; Yang, X. Surface Functionalization

- of Titanium Alloy with miR-29b Nanocapsules To Enhance Bone Regeneration. *ACS Appl. Mater. Interfaces* **2016**, *8*, 5783-5793.
- (20) Lai, J.-Y. Biocompatibility of chemically cross-linked gelatin hydrogels for ophthalmic use. *J. Mater. Sci. Mater. Med.* **2010**, *21*, 1899-1911.
- (21) Monteiro, I. P.; Shukla, A.; Marques, A. P.; Reis, R. L.; Hammond, P. T. Spray-assisted layer-by-layer assembly on hyaluronic acid scaffolds for skin tissue engineering. *J. Biomed. Mater. Res. A* **2015**, *103*, 330-340.
- (22) Lee, B. P.; Messersmith, P. B.; Israelachvili, J. N.; Waite, J. H. Mussel-inspired adhesives and coatings. *Annu. Rev. Mater. Res.* **2011**, *41*, 99.
- (23) Lee, H.; Scherer, N. F.; Messersmith, P. B. Single-molecule mechanics of mussel adhesion. *Proc. Natl. Acad. Sci. U.S.A.* **2006**, *103*, 12999-13003.
- (24) Lee, H.; Dellatore, S. M.; Miller, W. M.; Messersmith, P. B. Mussel-inspired surface chemistry for multifunctional coatings. *Science* **2007**, *318*, 426-430.
- (25) Lee, H.; Lee, B. P.; Messersmith, P. B. A reversible wet/dry adhesive inspired by mussels and geckos. *Nature* **2007**, *448*, 338-341.
- (26) Hong, S.; Pirovich, D.; Kilcoyne, A.; Huang, C.-H.; Lee, H.; Weissleder, R. Supramolecular Metallo-Bioadhesive for Minimally Invasive Use. *Adv. Mater.* **2016**, *28*, 8675-8680.
- (27) Cong, Y.; Xia, T.; Zou, M.; Li, Z.; Peng, B.; Guo, D.; Deng, Z. Mussel-inspired polydopamine coating as a versatile platform for synthesizing polystyrene/Ag nanocomposite particles with enhanced antibacterial activities. *J. Mater. Chem. B* **2014**, *2*, 3450-3461.
- (28) Sedó, J.; Saiz-Poseu, J.; Busqué, F.; Ruiz-Molina, D. Catechol-Based Biomimetic Functional Materials. *Adv. Mater.* **2013**, *25*, 653-701.
- (29) Liu, Y.; Ai, K.; Lu, L. Polydopamine and Its Derivative Materials: Synthesis and Promising Applications in Energy, Environmental, and Biomedical Fields. *Chem. Rev.* **2014**, *114*, 5057-5115.
- (30) Li, L.; Smitthipong, W.; Zeng, H. Mussel-inspired hydrogels for biomedical and environmental applications. *Polym. Chem.* **2015**, *6*, 353-358.
- (31) Stepuk, A.; Halter, J. G.; Schaetz, A.; Grass, R. N.; Stark, W. J. Mussel-inspired load bearing metal-polymer glues. *Chem. Commun.* **2012**, *48*, 6238-6240.
- (32) Bajaj, P.; Schweller, R. M.; Khademhosseini, A.; West, J. L.; Bashir, R. 3D biofabrication strategies for tissue engineering and regenerative medicine. *Annu. Rev. Biomed. Eng.* **2014**, *16*, 247.
- (33) Chen, Y. C.; Lin, R. Z.; Qi, H.; Yang, Y.; Bae, H.; Melero-Martin, J. M.; Khademhosseini, A. Functional human vascular network generated in photocrosslinkable gelatin methacrylate hydrogels. *Adv. Funct. Mater.* **2012**, *22*, 2027-2039.
- (34) Nichol, J. W.; Koshy, S. T.; Bae, H.; Hwang, C. M.; Yamanlar, S.; Khademhosseini, A. Cell-laden microengineered gelatin methacrylate hydrogels. *Biomaterials* **2010**, *31*, 5536-5544.
- (35) Ganesh, N.; Jayakumar, R.; Koyakutty, M.; Mony, U.; Nair, S. V. Embedded silica nanoparticles in poly (caprolactone) nanofibrous scaffolds enhanced osteogenic potential for bone tissue engineering. *Tissue Eng., Part A* **2012**, *18*, 1867-1881.
- (36) Gaharwar, A. K.; Kishore, V.; Rivera, C.; Bullock, W.; Wu, C. J.; Akkus, O.; Schmidt, G. Physically Crosslinked Nanocomposites from Silicate-Crosslinked PEO: Mechanical Properties and Osteogenic Differentiation of Human Mesenchymal Stem Cells. *Macromol. Biosci.* **2012**, *12*, 779-793.
- (37) Gaharwar, A. K.; Mihaila, S. M.; Swami, A.; Patel, A.; Sant, S.; Reis, R. L.; Marques, A. P.; Gomes, M. E.; Khademhosseini, A. Bioactive silicate nanoplatelets for osteogenic differentiation of human mesenchymal stem cells. *Adv. Mater.* **2013**, *25*, 3329-3336.
- (38) Loessner, D.; Meinert, C.; Kaemmerer, E.; Martine, L. C.; Yue, K.; Levett, P. A.; Klein, T. J.; Melchels, F. P.; Khademhosseini, A.; Hutmacher, D. W. Functionalization, preparation and use of cell-laden gelatin methacryloyl-based hydrogels as modular tissue culture platforms. *Nat. Protoc.* **2016**, *11*, 727-746.
- (39) Zhang, Y.-N.; Avery, R. K.; Vallmajo-Martin, Q.; Assmann, A.; Vegh, A.; Memic, A.; Olsen, B. D.; Annabi, N.;

- 1 Khademhosseini, A. A Highly Elastic and Rapidly Crosslinkable Elastin-Like Polypeptide-Based Hydrogel for  
2 Biomedical Applications. *Adv. Funct. Mater.* **2015**, *25*, 4814-4826.
- 3 (40) Shin, S. R.; Aghaei-Ghareh-Bolagh, B.; Dang, T. T.; Topkaya, S. N.; Gao, X.; Yang, S. Y.; Jung, S. M.; Oh, J. H.;  
4 Dokmeci, M. R.; Tang, X. S. Cell-laden Microengineered and Mechanically Tunable Hybrid Hydrogels of Gelatin and  
5 Graphene Oxide. *Adv. Mater.* **2013**, *25*, 6385-6391.
- 6 (41) Shin, H.; Olsen, B. D.; Khademhosseini, A. The mechanical properties and cytotoxicity of cell-laden  
7 double-network hydrogels based on photocrosslinkable gelatin and gellan gum biomacromolecules. *Biomaterials* **2012**,  
8 *33*, 3143-3152.
- 9 (42) Panzavolta, S.; Gioffrè, M.; Focarete, M. L.; Gualandi, C.; Foroni, L.; Bigi, A. Electrospun gelatin nanofibers:  
10 optimization of genipin cross-linking to preserve fiber morphology after exposure to water. *Acta Biomater.* **2011**, *7*,  
11 1702-1709.
- 12 (43) Jaiswal, A.; Chhabra, H.; Soni, V.; Bellare, J. Enhanced mechanical strength and biocompatibility of electrospun  
13 polycaprolactone-gelatin scaffold with surface deposited nano-hydroxyapatite. *Mater. Sci. Eng., C* **2013**, *33*,  
14 2376-2385.
- 15 (44) Liao, H.; Walboomers, X. F.; Habraken, W. J.; Zhang, Z.; Li, Y.; Grijpma, D. W.; Mikos, A. G.; Wolke, J. G.;  
16 Jansen, J. A. Injectable calcium phosphate cement with PLGA, gelatin and PTMC microspheres in a rabbit femoral  
17 defect. *Acta Biomater.* **2011**, *7*, 1752-1759.
- 18 (45) Yue, K.; Trujillo-de Santiago, G.; Alvarez, M. M.; Tamayol, A.; Annabi, N.; Khademhosseini, A. Synthesis,  
19 properties, and biomedical applications of gelatin methacryloyl (GelMA) hydrogels. *Biomaterials* **2015**, *73*, 254-271.
- 20 (46) Nikkhah, M.; Eshak, N.; Zorlutuna, P.; Annabi, N.; Castello, M.; Kim, K.; Dolatshahi-Pirouz, A.; Edalat, F.; Bae,  
21 H.; Yang, Y. Directed endothelial cell morphogenesis in micropatterned gelatin methacrylate hydrogels. *Biomaterials*  
22 **2012**, *33*, 9009-9018.
- 23 (47) Jia, W.; Gungor-Ozkerim, P. S.; Zhang, Y. S.; Yue, K.; Zhu, K.; Liu, W.; Pi, Q.; Byambaa, B.; Dokmeci, M. R.;  
24 Shin, S. R.; Khademhosseini, A. Direct 3D Bioprinting of Perfusible Vascular Constructs Using a Blend Bioink.  
25 *Biomaterials* **2016**, *106*, 58-68.
- 26 (48) Saxer, S.; Portmann, C.; Tosatti, S.; Gademann, K.; Zurcher, S.; Textor, M. Surface assembly of  
27 catechol-functionalized poly (l-lysine)-graft-poly (ethylene glycol) copolymer on titanium exploiting combined  
28 electrostatically driven self-organization and biomimetic strong adhesion. *Macromolecules* **2009**, *43*, 1050-1060.
- 29 (49) You, I.; Kang, S. M.; Byun, Y.; Lee, H. Enhancement of blood compatibility of poly (urethane) substrates by  
30 mussel-inspired adhesive heparin coating. *Bioconjugate Chem.* **2011**, *22*, 1264-1269.
- 31 (50) Zvarec, O.; Purushotham, S.; Masic, A.; Ramanujan, R. V.; Miserez, A. Catechol-functionalized chitosan/iron  
32 oxide nanoparticle composite inspired by mussel thread coating and squid beak interfacial chemistry. *Langmuir* **2013**,  
33 *29*, 10899-10906.
- 34 (51) Lee, H. J.; Koo, A. N.; Lee, S. W.; Lee, M. H.; Lee, S. C. Catechol-functionalized adhesive polymer nanoparticles  
35 for controlled local release of bone morphogenetic protein-2 from titanium surface. *J. Control. Release* **2013**, *170*,  
36 198-208.
- 37 (52) Kang, S. M.; Park, S.; Kim, D.; Park, S. Y.; Ruoff, R. S.; Lee, H. Simultaneous Reduction and Surface  
38 Functionalization of Graphene Oxide by Mussel-Inspired Chemistry. *Adv. Funct. Mater.* **2011**, *21*, 108-112.
- 39 (53) Salwiczek, M.; Qu, Y.; Gardiner, J.; Strugnell, R. A.; Lithgow, T.; McLean, K. M.; Thissen, H. Emerging rules for  
40 effective antimicrobial coatings. *Trends Biotechnol.* **2014**, *32*, 82-90.
- 41 (54) Cloutier, M.; Mantovani, D.; Rosei, F. Antibacterial Coatings: Challenges, Perspectives, and Opportunities.  
42 *Trends Biotechnol.* **2015**, *33*, 637-652.
- 43 (55) Mihaila, S. M.; Gaharwar, A. K.; Reis, R. L.; Khademhosseini, A.; Marques, A. P.; Gomes, M. E. The osteogenic  
44 differentiation of SSEA-4 sub-population of human adipose derived stem cells using silicate nanoplatelets.  
45 *Biomaterials* **2014**, *35*, 9087-9099.
- 46 (56) Xavier, J. R.; Thakur, T.; Desai, P.; Jaiswal, M. K.; Sears, N.; Cosgriff-Hernandez, E.; Kaunas, R.; Gaharwar, A.  
47 K. Bioactive nanoengineered hydrogels for bone tissue engineering: a growth-factor-free approach. *ACS Nano* **2015**, *9*,  
48  
49  
50  
51  
52  
53  
54  
55  
56  
57  
58  
59  
60

1 3109-3118.

2  
3 (57) Trappmann, B.; Gautrot, J. E.; Connelly, J. T.; Strange, D. G.; Li, Y.; Oyen, M. L.; Stuart, M. A. C.; Boehm, H.;  
4 Li, B.; Vogel, V. Extracellular-matrix tethering regulates stem-cell fate. *Nature Mater.* **2012**, *11*, 642-649.

5 (58) Engler, A. J.; Griffin, M. A.; Sen, S.; Bönnemann, C. G.; Sweeney, H. L.; Discher, D. E. Myotubes differentiate  
6 optimally on substrates with tissue-like stiffness: pathological implications for soft or stiff microenvironments. *J. Cell*  
7 *Biol.* **2004**, *166*, 877-887.

8  
9 (59) Rupp, F.; Scheideler, L.; Olshanska, N.; de Wild, M.; Wieland, M.; Geis-Gerstorfer, J. Enhancing surface free  
10 energy and hydrophilicity through chemical modification of microstructured titanium implant surfaces. *J. Biomed.*  
11 *Mater. Res. A* **2006**, *76A*, 323-334.

12 (60) Annabi, N.; Shin, S. R.; Tamayol, A.; Miscuglio, M.; Bakooshi, M. A.; Assmann, A.; Mostafalu, P.; Sun, J.-Y.;  
13 Mithieux, S.; Cheung, L.; Tang, X.; Weiss, A. S.; Khademhosseini, A. Highly Elastic and Conductive Human-Based  
14 Protein Hybrid Hydrogels. *Adv. Mater.* **2016**, *28*, 40-49.

15 (61) Gong, J. P. Why are double network hydrogels so tough? *Soft Matter* **2010**, *6*, 2583-2590.

16  
17 (62) Hilpert, K.; Elliott, M.; Jenssen, H.; Kindrachuk, J.; Fjell, C. D.; Körner, J.; Winkler, D. F. H.; Weaver, L. L.;  
18 Henklein, P.; Ulrich, A. S.; Chiang, S. H. Y.; Farmer, S. W.; Pante, N.; Volkmer, R.; Hancock, R. E. W. Screening and  
19 Characterization of Surface-Tethered Cationic Peptides for Antimicrobial Activity. *Chem. Biol.* **2009**, *16*, 58-69.

20 (63) Boulos, L.; Prévost, M.; Barbeau, B.; Coallier, J.; Desjardins, R. LIVE/DEAD® BacLight™: application of a  
21 new rapid staining method for direct enumeration of viable and total bacteria in drinking water. *J. Microbiol. Methods*  
22 **1999**, *37*, 77-86.

23 (64) Zhao, L.; Chu, P. K.; Zhang, Y.; Wu, Z. Antibacterial coatings on titanium implants. *J. Biomed. Mater. Res. B*  
24 **2009**, *91B*, 470-480.

25 (65) Pagel, M.; Hassert, R.; John, T.; Braun, K.; Wießler, M.; Abel, B.; Beck-Sickinger, A. G. Multifunctional Coating  
26 Improves Cell Adhesion on Titanium by using Cooperatively Acting Peptides. *Angew. Chem., Int. Ed.* **2016**, *55*,  
27 4826-4830.

28 (66) Goodman, S. B.; Yao, Z.; Keeney, M.; Yang, F. The future of biologic coatings for orthopaedic implants.  
29 *Biomaterials* **2013**, *34*, 3174-3183.

30 (67) Bose, S.; Fielding, G.; Tarafder, S.; Bandyopadhyay, A. Understanding of dopant-induced osteogenesis and  
31 angiogenesis in calcium phosphate ceramics. *Trends Biotechnol.* **2013**, *31*, 594-605.

32 (68) Qin, X.; Jiang, Q.; Matsuo, Y.; Kawane, T.; Komori, H.; Moriishi, T.; Taniuchi, I.; Ito, K.; Kawai, Y.; Rokutanda,  
33 S. Cbfb regulates bone development by stabilizing Runx family proteins. *J. Bone Miner. Res.* **2015**, *30*, 706-714.

34 (69) Ricarte, F.; Nakatani, T.; Partridge, N. PTH Signaling and Epigenetic Control of Bone Remodeling. *Curr. Mol.*  
35 *Biol. Rep.* **2016**, *2*, 56-61.

36 (70) Raphael, J.; Holodniy, M.; Goodman, S. B.; Heilshorn, S. C. Multifunctional coatings to simultaneously promote  
37 osseointegration and prevent infection of orthopaedic implants. *Biomaterials* **2016**, *84*, 301-314.

## TOC Graph

